NASA TN D-286

$7N-20$
$198709$
$P-42$

# NASA

# TECHNICAL NOTE

## D-286

COMPARISON OF LOCALIZED HEAT-TRANSFER RATES IN A LIQUID-

OXYGEN - HEPTANE ROCKET ENGINE EMPLOYING SEVERAL

INJECTION METHODS AND OXIDANT-FUEL RATIOS

By Richard F. Neu

Lewis Research Center
Cleveland, Ohio

NATIONAL AERONAUTICS AND SPACE ADMINISTRATION

WASHINGTON                    June 1960

NATIONAL AERONAUTICS AND SPACE ADMINISTRATION

TECHNICAL NOTE D-286

COMPARISON OF LOCALIZED HEAT-TRANSFER RATES IN A LIQUID-

OXYGEN - HEPTANE ROCKET ENGINE EMPLOYING SEVERAL

INJECTION METHODS AND OXIDANT-FUEL RATIOS

By Richard F. Neu

SUMMARY

The effects of injection process and oxidant-fuel ratio upon local values of heat transfer were studied in an 1800-pound-thrust rocket engine. The solid-wall rocket engine was constructed with thermocouples buried in thermally isolated segments of the wall. Local values of heat transfer were obtained by applying transient temperature data to an approximate solution of the transient conduction equation.

The propellants used were liquid oxygen and heptane, and the oxidant-fuel-ratio range was 1.2 to 3.6. Two basic injection methods were investigated: parallel sheets of each propellant directed downstream, and triplet impingement of both propellants to form mixed sprays.

Circumferential variations in local heat flux as high as 2:1 were observed. These heat-flux variations were influenced by the injector type and the oxidant-fuel ratio. Within the chamber, the longitudinal variations of heat flux were smaller, generally, than the circumferential variations.

Each experimental case is explained individually in terms of such factors as injector spray pattern, spatial heat release, and patterns of hot gas flow. No general model is proffered that explains these distributions of local heat flux for the different injectors and operating conditions.

INTRODUCTION

This report is concerned with the effect of injector design and oxidant-fuel ratio upon localized heat-transfer rates in a rocket engine. These local rates were determined from time-temperature records in a solid-copper-wall high-heat-capacitance engine. This engine was segmented

in such a manner that both circumferential and longitudinal heat-transfer variations could be studied. Because of symmetry only half the isolated segments were instrumented so that the local transient heat transfer could be determined.

With the exception of one test condition, the tests were conducted at a nominal thrust of 1800 pounds; the propellants were heptane and liquid oxygen. Two basic injector types were examined: parallel-sheet and triplet (ref. 1). For each principal injector configuration three oxidant-fuel mixture ratios were examined.

Local heat-flux rates were observed during systematic variations of injection pattern and oxidant-fuel ratio. The variations in heat flux were studied in terms of the injection spray pattern, spatial configurations of the combustion, and secondary flows of the combustion products.

<center>APPARATUS AND PROCEDURE</center>

The apparatus comprises various injectors, a solid-wall rocket chamber and nozzle, and instrumentation to indicate heat-transfer rates and overall rocket performance.

<center>Injectors</center>

Parallel-sheet injectors. - The performance of the parallel-sheet injectors was investigated in a previous study and reported in reference 1. Various configurations were obtained from an injector body with rotatable and removable inserts (fig. 1), each insert having a nominal thrust of 200 pounds. The detail of these elements is shown in figure 2. Each insert had four deflector plates which were located and shaped to produce two oxidant sprays and one fuel spray. All sprays were mutually parallel and perpendicular to the injector face.

Parallel-sheet injectors with nine elements were investigated in two orientations: the butt (fig. 3) and the 12° (fig. 4). Both of these injector configurations were examined during the injection study of reference 1. For the butt orientation, the intersection of the edges of adjacent propellant sprays produced a coalescence of like propellants. This coalescence adversely affected overall rocket performance and induced zones of nonuniform heat release in the combustion chamber.

In the 12° orientation, the fantails of unlike propellants intersected to enhance the injection process. This injector was better than the butt configuration with respect to overall performance and uniformity of heat release.

In addition, a modified butt orientation of four elements was investigated. Five inner elements were removed and replaced by blank inserts.

Nine-element triplet injectors. - Two triplet[1] injectors were investigated. One consisted of nine elements fixed in the butt orientation (fig. 5). This injector (previously examined in ref. 1), and others similar to it, gave evidence of high heat transfer near the injector face. Consequently, an appreciable gradient in longitudinal heat flux might be expected. The relatively high characteristic velocity of this injector (ref. 1) would produce higher heat-transfer rates than the parallel sheets.

The interelement spacing and location of the elements in this nine-unit triplet injector were the same as those of the parallel-sheet butt-orientation injector (fig. 3). For the triplet, the zones of interference between adjacent fantails were composed of mixed propellants, whereas for the parallel sheets, the interference involved previously unmixed propellants. Therefore, although the orientation of the elements was identical, one injector displayed maximum interference between like propellant sprays (parallel-sheet), while the other exhibited maximum interference between mixed propellant sprays (triplet).

Single-element triplet injector. - This injector consisted of one large 1600-pound-thrust unit (fig. 6). Although preliminary tests with this injector showed relatively poor performance, studies of the localized heat flux with a single element were considered pertinent to an evaluation of the local heat-transfer problem.

Rocket Chamber and Nozzle

The solid-copper rocket engine diagramed in figure 7, which consisted of a chamber section and a nozzle section, was designed for a nominal thrust level of 1800 pounds at a chamber pressure of 300 pounds per square inch. The chamber inside diameter was 6 inches, and the wall thickness was $1\frac{1}{4}$ inches. The overall engine length (chamber plus nozzle) was 11 inches. No nozzle divergence section was used. The throat diameter was 2.42 inches, and the contraction ratio was 6.15. Propellants were ignited by a 3/8-inch sparkplug located in the injector face.

To isolate the local heat-transfer effects, the engine was slotted circumferentially and longitudinally. There were a total of 44 engine segments, 28 segments in the chamber and 16 in the nozzle.

---

[1]Called "impinging-jets" injector in ref. 1. The name was changed to "triplet" to prevent confusion between the process mentioned here and the one which features impingement of two unlike propellant jets.

## Instrumentation

Heat transfer. - Because the injection pattern of each of the injectors was symmetrical about a pair of orthogonal axes, only one-half (two adjacent longitudinal rows) of the engine segments was instrumented. The design of each injector was such that, by proper positioning of the chamber, one longitudinal row of instrumented segments (hereafter referred to as spray wall segments) received the maximum amount of propellant spray impingement, and the other row, displaced $90^\circ$ from the first (hereafter referred to as nonspray wall segments), received a minimum amount. It was assumed that this method of thermocouple location would indicate the maximum and minimum circumferential heat flux attributable to spray impingement. In order to check whether maximum and minimum heat-flux conditions were being observed, the engine was rotated $45^\circ$ so that the instrumented segments would be equally influenced by the sprays. This procedure was followed for the parallel-sheet and single-unit triplet injectors.

A thermocouple was placed in the geometric center of each instrumented chamber section midway between the gas-side and outside walls (5/8 in. from both walls). This distance from the gas-side wall to the thermocouple location was maintained in the nozzle even though the wall thickness was greater in this region to accommodate the larger heat loads. The cold junction of each thermocouple was located in a common bath of melting ice.

The 22 thermocouple temperatures were recorded on six channels of a recording oscillograph. The thermocouple lead wires and oscillograph channel leads were connected to a 100-point selector switch which revolved at a rate that recorded the voltage of each thermocouple for 0.15 second at intervals of 0.5 to 1 second.

Rocket performance. - The injector performance is reported in terms of the characteristic velocity $c^*$. The evaluation of this parameter involves measurement of the chamber pressure and the propellant flow rates. A strain-gage type transducer located in the chamber wall near the injector face was used to measure chamber pressure. Propellant flow rates were measured by turbine-type flowmeters. Thrust measurements were not made.

## Procedure

Local heat-flux values $q$ and characteristic velocity $c^*$ were determined over a range of oxidant-fuel ratio $O/F$ (1.2 to 3.6) for all injectors except the parallel-sheet in the $12^\circ$ orientation and four-element configurations. These exceptions were studied at peak $O/F$ only. Table I summarizes the injector configurations used. Each rocket firing

lasted about 3.5 seconds with full propellant flows and chamber pressure being maintained constant for about 3 seconds.

## HEAT-FLUX CALCULATIONS

The transient method of reference 2 was used to compute the localized heat-transfer values. Each engine segment was considered as an independent heat capacitor experiencing local transient heat transfer.

The energy balance on a segment may be expressed as $\quad q = -\dfrac{W}{A} c_p \dfrac{dT}{d\theta}$
where

q    rate of heat flux per unit area, Btu/(sq in.)(sec)

W    weight of segment, lb

A    segment inner area, sq in.

$c_p$    specific heat of segment, Btu/(lb)($^{\circ}$F)

$\dfrac{dT}{d\theta}$    rate of change of segment average temperature with respect to time, $^{\circ}$F/sec

W and A are measured values. The $c_p$ value at the segment average temperature was used and was calculated from $c_p = 5.44 + 0.001462\ T$ (ref. 3). The term $dT/d\theta$ is the slope of the tangent to the temperature-time curve of the segment thermocouple. The slope was calculated at the third second of operation. Longer operation of the engine might have damaged the injector and allowed an appreciable heat loss from the outer walls of the chamber.

## INFLUENCING FACTORS IN ROCKET-ENGINE HEAT TRANSFER

The heat-transfer mechanism from the combustion gases to the walls of a rocket engine can be subdivided into two submechanisms. One is the reacting system which produces the enthalpy for driving the heat transfer. The other is the heat transport mechanism through the thermal boundary layer which is dependent on the local fluid velocity and such properties as density, specific heat, thermal conductivity, and viscosity.

### Reacting System

The reacting system will be considered insofar as it affects the O/F of the products of combustion. Reference 4 indicates that the propellants must be in the vaporized state before they enter into the

combustion process. The author hypothesized, therefore, that the vaporization rate of the less volatile propellant is the controlling factor in the combustion process rate. Table II, taken from reference 5 (fig. 1(d)) discloses that, for comparable drop sizes and velocities, the liquid oxygen vaporizes much more rapidly than the heptane under rocket firing conditions. If it is assumed that the propellants react stoichiometrically, then the O/F of the remaining gaseous products (combustion products plus unreacted vaporized oxidant) will be higher than the O/F calculated from the propellant flow rates. It is apparent (table II) that this O/F variation is not constant but that it varies axially through the rocket engine. For the sake of simplicity, however, it is sufficient to state qualitatively that the O/F of the gaseous products is always greater than the measured liquid O/F.

### Heat Transport Mechanism

For forced-convection heat transfer to various surface geometries, it has been shown that the heat-transfer coefficient can be computed from the following general equation

$$\frac{hD}{k} = C_1 Re^m Pr^n$$

where h is the heat-transfer coefficient, D is the diameter of the tube, k is thermal conductivity, Re is Reynolds number, and Pr is Prandtl number. The appropriate values of the constants C, m, and n are presented in the literature.

An analysis of this type of correlation as it pertains to the thermal boundary layer in a rocket engine appears in the appendix. In this derivation the heat-transfer coefficient h is shown to be influenced most by the local values of mass velocity $G^m$ and thermal conductivity k as follows:

$$h \sim C_2 G^m k \tag{1}$$

where $C_2$ is a constant. Since $q = h \Delta T$,

$$q \sim G^m k T_g \tag{2}$$

where $T_g$ is combustion gas temperature. The effects of changes in O/F or chamber pressure are reflected in mass flow and thermal conductivity in equation (2).

## Other Factors Affecting Heat Transfer

A spray (liquid or gaseous) of a nonburning propellant would have a tendency to cool the region affected by the spray. Conversely, sprays of burning propellants tend to increase the heat flux in that region.

## DISCUSSION OF RESULTS

Local heat-transfer rates for various circumferential and longitudinal locations in the rocket chamber and nozzle are presented in figures 8 to 17. For all the experimental runs, the third second of rocket operation was chosen as the time to compute these heat-flux rates. Varying the circumferential location of the thermocouples, the injector pattern, or the O/F produced the results presented in these figures. Each figure is labeled as to the injector pattern, and the schematic drawings show the circumferential and longitudinal locations of the thermocouples with respect to the injector.

To facilitate the discussion of the local heat-transfer results, a system was devised for labeling the various injector configurations and the circumferential location of the thermocouples. This system is summarized in tables I and III. Note that each of figures 8 to 17 contains heat-transfer data from two injector patterns; there is a reference case and a variation of the reference case. The "reference" and "variation" cases are indicated in table I.

## Parallel-Sheet Injectors

Heat-flux results obtained from a group of injectors employing parallel-sheet inserts in the butt orientation are shown in figures 8 to 11. The reference case is labeled case I and those compared are cases II, III, IV, and V; they are described in table I. With the exception of case II, which is a check on instrumentation, all the parallel-sheet butt-orientation injectors exhibited large circumferential heat-flux variations near the injector. The percent perturbation in the circumferential distribution of the heat flux appeared relatively constant over the O/F range investigated.

Case I. - In case I (figs. 8 to 12) nine injector elements were butt-oriented and run at peak-performance O/F. The heat-transfer results from this case (solid curves) indicate almost a 2:1 variation in circumferential heat transfer near the injector; the higher local heat-transfer rates were located at the nonspray wall segments. Localized high gas velocities probably caused the augmented heat transfer. To explain, it is assumed that the combustion zone is confined to that volume occupied by propellant spray in the following sketch:

Nonspray thermocouples

Injector elements

Sprays

Combustion zone (inside heavy lines)

Chamber
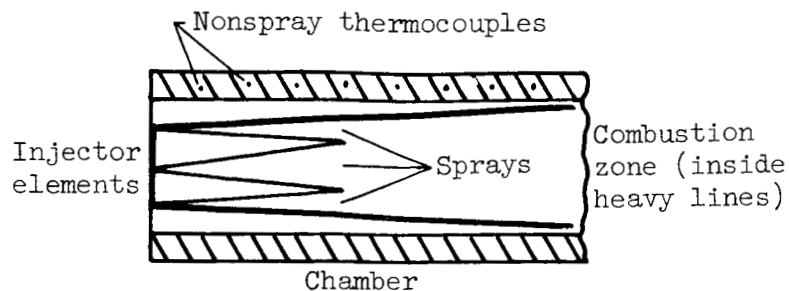
(a)

The combustion zone is a source of hot burned gases. Because of continuity requirements, the hot gases tend to fill the voids above and below the combustion zone as shown in the following two-dimensional view, looking upstream from the nozzle:

Voids

Hot gas flow
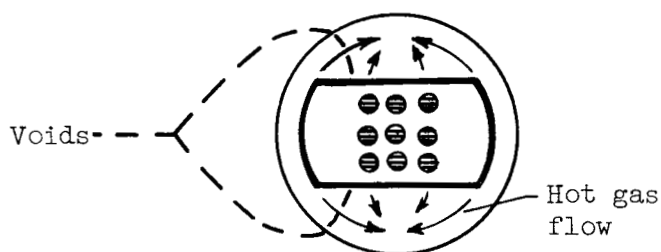
(b)

This process, of course, is occurring down the whole length of the chamber. In addition, as the gases reach the outer extremities of these voids, they probably change direction and head downstream (in the third dimension) toward the nozzle as follows:

Hot gas flow
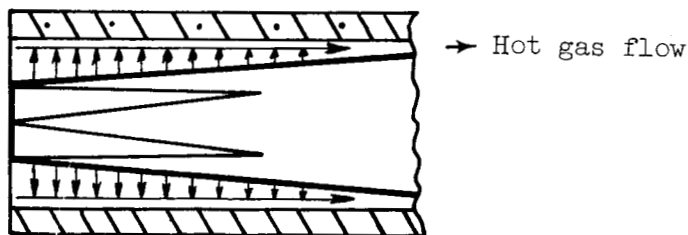
(c)

This three-dimensional effect was previously noticed in gas flow patterns in high-speed photographs taken of single-element injectors (fig. 6(c) of ref. 6). Although the injection process and number of elements in the referenced case were dissimilar to those of this nine-element case, the chamber cross-sectional injection patterns were similar. In each case two voids outside the combustion zone located about 180° apart (as seen in sketch (b)) were present. The turbulence of these burned gases was probably very high near the nonspray wall segments and thus tended to increase the heat transfer in this vicinity (see eq. (1)).

The spray wall segments exhibited the minimum local heat-transfer rate. The impingement of unburned propellants effectively film-cooled these surfaces. However, as these propellants moved downstream, they mixed and burned. Their cooling capacity decreased until, at the throat, the heat flux levels of the spray and nonspray wall segments were approximately equal.

Case II. - For case II (fig. 8) the rocket chamber was rotated 45° from the case I chamber-injector orientation so that both rows of instrumented segments were equally affected by the spray patterns. As shown in figure 8, the heat-flux levels of each segment were comparable but were less than the averages of the high and low values observed in case I. Consequently, it is concluded that each segment thermocouple is sensing a somewhat local heat flux rather than some average value for the entire segment.

For the purpose of determining gross variations in heat flux this instrumentation suffices. Also, the instrument locations of case I appear to produce approximately maximum and minimum heat-flux values.

Case III. - The injector configuration of case III (fig. 9) is quite similar to that in case I except that five elements are replaced by blanks (see schematic drawings in fig. 9). This caused a decrease in the total propellant flow rate and chamber pressure.

Circumferential variations of heat flux, similar to those in case I, are also present in case III. For case III, however, it appears that these variations persist downstream. It appears that the decrease in total propellant flow rate and the wider spacing of the injector elements for case III decreased the mixing; that is, at any given distance from the injector face, the propellants in case I are more thoroughly mixed than they are in case III.

The general heat-flux levels (spray and nonspray) in case III are substantially lower than the corresponding levels in case I. This decrease can be attributed to the lower mass velocities (eq. (2)).

Case IV. - Case IV (fig. 10) is identical to case I except that a low O/F (about 1.2) was employed, whereas case I was run at peak O/F conditions.

For case IV circumferential heat-flux variations are present as in case I and can be explained as they were in case I. In case IV, however, these variations persist downstream, contrary to the results from case I. This can be explained if the O/F of the sprays hitting the engine wall in case IV is considered. Since the O/F is low, an excess of fuel is present in these sprays. Since there is an excess of fuel, a substantial amount of that fuel is not consumed or burned in the combustion process

and is available for film-cooling purposes downstream. In fact, the cooling continues through the throat itself so that the variation in circumferential heat flux is maintained.

Case V. - Case V (fig. 11) is identical to case I except that case V was run at a high mixture ratio (O/F of about 3.6). Again, circumferential heat-flux variations are present and can be explained as they were for case I. Because case V was run rich in oxidant, an ample amount of excess oxygen is available for downstream cooling of the spray wall segments. The oxidant vaporizes readily into a gas and thus it can mix more readily with the combustion products, so that once again downstream turbulence, or mixing, gradually diminishes and eventually eliminates the circumferential variations.

Case VI. - Case VI (fig. 12) is the only case involving parallel-sheet injectors in which the butt orientation is not used. Instead, the $12^\circ$ orientation, which features interference of unlike sprays, is used. This case was run at peak O/F for comparison with case I (nine-element parallel sheets, butt orientation).

The results for case VI indicate a rather uniform circumferential distribution of heat flux; the magnitude in the chamber section was between the maximum and minimum established in case I. The better mixing of oxidant and fuel sprays and the comparative absence of propellant drop coalescence (fig. 5(c) of ref. 1) probably resulted in more uniform burning within the combustion zone and, hence, more uniform circumferential heat patterns. The "hot" and "cold" spots of case I have apparently been thereby eliminated.

Nine-Element Triplet Injector

Heat-flux results obtained from the nine-element triplet injector are presented in cases VII to IX (figs. 13 to 15). One of the more obvious results from examining these figures is that the variation in circumferential heat flux is very sensitive to O/F. Such was not the case for the parallel-sheet injector. Also the general level of heat flux was greater for the nine-element triplet than for the parallel sheets when the comparison is made at peak O/F (fig. 13). The higher value of $c^*$ for this configuration indicates a higher combustion temperature and therefore a higher heat flux.

Case VII. - The magnitude of the circumferential heat-flux variation and the rate of its attentuation down the length of the chamber appear similar to that of the nine-element parallel-sheet injector at peak O/F (fig. 13). However, there is an important difference between the heat-transfer results of these two injectors. In case VII the highest heat flux is present in the spray wall segments, while the nonspray wall

segments are the hottest in the case of the parallel-sheet injector. This difference can be explained in terms of the spray patterns.

Sprays emanating from the parallel-sheet elements contain only one propellant. As a result, the spray is not burning and it cools the wall adjacent to it. The sprays from the triplet inserts contain both propellants and they are mixed and burning. They tend to heat the wall adjacent to them. It should be noted that the nonspray wall segments in this case are also heated by the reacting propellant sprays. Figure 5 shows evidence of secondary sprays (dashed arrows) which result from interference of the primary sprays (solid arrows). The spray wall segments, however, are affected by a greater number of these heat-release zones (fig. 5), which explains why the spray wall segments exhibit the higher heat flux.

Also, the heat-release zones that project into the vicinity of the nonspray wall segments occupy much of the two large "void" regions that were present in the cases involving the parallel-sheet butt-orientation injectors. Consequently, no appreciable secondary flows are present in the vicinity of the nonspray wall segments to increase the heat-transfer rate as in the cases involving the parallel-sheet injectors.

Cases VIII and IX. - In cases VIII (fig. 14, low O/F) and IX (fig. 15, high O/F) the circumferential variation in heat flux has practically disappeared. Also the general level of heat transfer has dropped considerably from the level of case VII (peak O/F). These results can be explained if the measured liquid O/F of each case is considered.

Each heat-release zone emanates from some portion of a propellant spray. For the low O/F case, an excess of fuel is probably present in each spray. This excess would tend to cool the wall segments being directly affected by the spray, or, extending the reasoning further, the cooling of the wall segments by the excess fuel offsets much of the heat released from the heat-release zone. For the high O/F case, a similar situation prevails except that an excess of oxidant is the cooling agent.

Another general observation can be made when the results of the nine-unit triplet and the parallel sheets are compared. Near the injector face, the longitudinal distribution of heat flux on the wall has definite gradients for the triplet injectors, whereas, for the parallel sheets, no appreciable gradients are observed. Moreover, the slope of this gradient in the triplet curves is positive or negative depending on the O/F value. For example, in the low O/F case (VIII), the heat flux near the injector face is higher than it is farther downstream in the chamber. The situation is reversed in the high O/F case (IX), where the heat flux near the injector is less than it is downstream.

These longitudinal gradients can be related to local values of O/F near the injector face. Both the heat-release rate in the combustion

zone and the heat-transfer characteristics of the thermal boundary layer are O/F dependent. The local heat-release rate is appreciably reduced at either the high or low O/F condition.

Considering the thermal layer, equation (2) shows that the magnitude of the heat transport through the layer is a function of the thermal conductivity. From table II it is apparent that, regardless of the measured O/F, the O/F of the gaseous products (combustion products plus unreacted vaporized oxidant) near the injector face is always substantially higher than the measured O/F because the oxidant vaporizes at a much faster rate than the fuel. As the propellants move downstream, the percent of vaporized heptane approaches the percent of vaporized oxygen, and this produces a gradual reduction of the gaseous products O/F with chamber length. As a result,

(1) When the measured O/F is low, the local O/F of the gaseous products is relatively high near the injector face. According to figure 18, the thermal conductivity k is to the left of but probably rather close to the maximum point, and a rather high heat flux in this region (eq. (2)) results. Therefore, as the O/F of the gaseous products decreases with chamber length, k also decreases, and ultimately produces a gradual decrease in heat flux with chamber length.

(2) When the measured O/F is high, however, the still higher O/F of the gaseous products near the injector face places thermal conductivity k far to the right of the maximum point, and a relatively low heat flux in this vicinity results. The decrease in the O/F of gaseous products with chamber length in this case results in an increase in heat flux because thermal conductivity is gradually increasing.

## Single-Unit Triplet Injector

Heat-flux results obtained from the single-unit triplet injector are presented in figures 16 and 17. Cases X, XI, and XII are the peak, low, and high O/F runs, respectively.

From inspection of figures 16 and 17, it is apparent that the heat flux of the spray wall segments remained approximately constant over a range of O/F. In contrast, the heat flux of the nonspray walls fluctuated appreciably with O/F.

Apparently the local O/F and velocities at the edges of the spray were relatively constant as the overall O/F was varied. Thus the heat transfer to the spray wall segments was invarient.

The changes in average combustion temperature and average gas velocity with overall O/F are reflected in the widely changing heat flux of the nonspray wall segments.

The heat-transfer results from the single-element triplet show similarities to the results with the multiunit triplet in that the maximum heat flux for both occurs at peak $O/F$, and the heat transfer near the injector face varied inversely with the $O/F$. The latter result is peculiar to the triplet only and is not evident with the parallel-sheet injector.

## SUMMARY OF RESULTS

The most important observations which have evolved from this investigation of the effect of the injection process (parallel-sheet or triplet injectors) on local values of heat transfer in a rocket engine are as follows:

Two configurations of parallel-sheet injectors were involved in the test program; in one, the fantails of the propellant sprays butted, while in the other, the fantails were skewed $12^\circ$. The former configuration featured interference of like propellant sprays, while unlike propellant spray interference was present in the latter. For the butted-spray configuration, a 2:1 circumferential variation in heat flux was evident. The portion of the chamber wall that experienced spray impingement of unmixed propellants had the lowest heat-transfer rate. Approximately the same percentage of heat-flux variation occurred at all oxidant-fuel ratios for this injector. The large variations in circumferential heat flux were almost absent for the $12^\circ$ fantail orientation. The general performance level (characteristic velocity) was somewhat greater than that for the butt orientation.

Two triplet injectors were tested; one was a nine-element injector, the other was a single-element injector. Similarly to the parallel-sheet injector, the nine-element triplet showed a 2:1 circumferential variation of heat flux. Unlike results in the parallel-sheet injector, the percentage of heat-flux variation in the triplet varied with oxidant-fuel ratio and the hotter walls experienced spray impingement of mixed burning propellants. The maximum variation appeared at peak oxidant-fuel ratio. There was evidence of a longitudinal heat-flux gradient along the wall near the injector face. No such gradient was evident with the parallel sheets. For the triplet, the slope of the gradient was dependent on oxidant-fuel ratio.

For the single-element triplet, the heat flux of the spray wall segments remained substantially constant over a range of oxidant-fuel ratio. However, the heat flux of the nonspray wall segments fluctuated greatly with oxidant-fuel ratio.

The following applies to both injector types: As predicted from a simple heat-transfer analysis, the average heat flux varied with propellant mass-flow rate and combustion temperature. Since characteristic velocity and combustion temperature are related, the better performing injector (high characteristic velocity) exhibited the higher heat flux.

In the chamber the circumferential variations in heat flux were greater than the longitudinal.

No general mechanism or model explains the local distributions of heat flux for the different injectors and operating conditions. Each case must be explained individually in terms of such factors as injection spray pattern, spatial heat release in the combustor, and patterns of hot gas flow.

Lewis Research Center
    National Aeronautics and Space Administration
        Cleveland, Ohio, March 2, 1960

## APPENDIX - FACTORS THAT INFLUENCE THE

## HEAT-TRANSFER COEFFICIENT

For fully developed turbulent flow in a tube reference 7 shows that the heat-transfer coefficient can be related to the fluid properties and velocity through Colburn's dimensionless correlation:

$$\frac{hD}{k} = 0.023\left(\frac{DG}{\mu}\right)^{0.8}\left(\frac{c_p\mu}{k}\right)^{0.33}$$

where

h    heat-transfer coefficient

D    diameter of tube

k    thermal conductivity

G    mass velocity

$\mu$    viscosity

$c_p$    specific heat

Regrouping gives

$$h = \frac{k}{D}\ (0.023)\left(\frac{DG}{\mu}\right)^{0.8}\left(\frac{c_p\mu}{k}\right)^{0.33} \tag{3}$$

This relation may be applied to a rocket engine if the engine is considered to be a pipe. The significance of this application is to point out the important variables that control the heat flux into the walls of a rocket engine. The characteristic dimension  D  then becomes the chamber or nozzle diameter. Since all experimental runs were obtained from the same engine, D  remains constant and

$$h \sim \frac{G^{0.8}k^{0.67}c_p^{0.33}}{\mu^{0.47}}$$

or

$$h \sim \frac{G^{0.8}\mu^{0.2}c_p}{\left(\frac{c_p\mu}{k}\right)^{0.67}} \tag{4}$$

where  $c_p\mu/k = Pr$.

Theoretical values of $k$, $\mu$, and $c_p$ for the products of combustion of heptane with liquid oxygen are plotted against oxidant-fuel ratio $O/F$ in figures 18 to 20. These curves were obtained from unpublished NASA data. From figure 20, it can be seen that $\mu$ varies about 10 percent over the $O/F$ range 2.0 to 5.0. The variation between $O/F$ = 1.2 and 2.0 appears to be negligible (extrapolation of table III of ref. 8). There-fore, the variation in $\mu^{0.2}$ over the range $O/F$ = 1.2 to 5.0 is very small. Also, the variations in $c_p$ and $k$ over that range are such that the variation in $(c_p\mu/k)^{0.67}$ is also very small (about 1.5 percent). It should be emphasized at this point that the heat-flux changes encoun-tered in this investigation are about 25 to 75 percent of a mean value. Compared with these large changes, the variations in the expressions $\mu^{0.2}$ and $Pr^{0.67}$ with $O/F$ are negligible, and thus

$$h \sim G^{0.8}c_p \tag{5}$$

Since $q = h(T_g - T_w)$, where $q$ is heat flux, $T_g$ is combustion gas tem-perature, and $T_w$ is rocket inside wall temperature,

$$q \sim G^{0.8}c_p(T_g - T_w) \tag{6}$$

Theoretical $T_g$ values are plotted against $O/F$ (also obtained from unpublished NASA data) in figure 21. Values of $T_w$ for each case are shown in table IV. They were calculated by the method presented in ref-erence 9. Generally speaking, the values of $T_w$ are negligible compared with $T_g$, so that relation (6) simplifies to

$$q \sim G^{0.8}c_pT_g \tag{7}$$

Since $c_p$ and $k$ have similar variations with $O/F$ over the range of $O/F$ examined, relation (7) can be written as

$$q \sim G^{0.8}kT_g \tag{2}$$

which is the relation presented in the text of this report. This rela-tion can be applied to the overall rocket engine or to any localized portion of it.

REFERENCES

1. Neu, Richard F.:  Injection Principles for Liquid Oxygen and Heptane Using Nine-Element Injectors in an 1800-Pound-Thrust Rocket Engine. NACA RM E57E13, 1957.

2. Greenfield, Stanley:  Determination of Rocket-Motor Heat-Transfer Coefficients by the Transient Method.  Jour. Aero. Sci., vol. 18, no. 8, Aug. 1951, pp. 512-518; 526.

3. Perry, John H.:  Chemical Engineers' Handbook.  Third ed., McGraw-Hill Book Co., Inc., 1950, p. 220.

4. Priem, Richard J.:  Propellant Vaporization as a Criterion for Rocket-Engine Design; Calculations of Chamber Length to Vaporize a Single n-Heptane Drop.  NACA TN 3985, 1957.

5. Priem, Richard J.:  Propellant Vaporization as a Criterion for Rocket-Engine Design; Calculations of Chamber Length to Vaporize Various Propellants.  NACA TN 3883, 1958.

6. Heidmann, M. F., and Auble, C. M.:  Injection Principles from Combustion Studies in a 200-Pound-Thrust Rocket Engine Using Liquid Oxygen and Heptane.  NACA RM E55C22, 1955.

7. McAdams, William H.:  Heat Transmission.  Third ed., McGraw-Hill Book Co., Inc., 1954, p. 219.

8. Huff, Vearl N., Fortini, Anthony, and Gordon, Sanford:  Theoretical Performance of JP-4 Fuel and Liquid Oxygen as a Rocket Propellant. II - Equilibrium Composition.  NACA RM E56D23, 1956.

9. Hatch, James E., Schacht, Ralph L., Albers, Lynn U., and Saper, Paul G.: Graphical Presentation of Difference Solution for Transient Radial Heat Conduction in Hollow Cylinders with Heat Transfer at the Inner Radius and Finite Slabs with Heat Transfer at One Boundary.  NASA TR R-56, 1960.

E-573

CG-3

TABLE I. - INJECTOR CONFIGURATIONS AND THERMOCOUPLE LOCATIONS

| Case | Basic injector type | Figure | Sketch | Description | Reference or variation case | Oxidant-fuel ratio, O/F | Thermocouple row orientations |
|---|---|---|---|---|---|---|---|
| I | Parallel-sheet | 8 to 13 | | Butt orientation, nine elements | Reference | Peak | Maximum and minimum heat transfer |
| II | | 8 | | | Variation | Peak | Mean heat transfer |
| III | Parallel-sheet | 9 | | Butt orientation, four elements | Variation | Peak | Maximum and minimum heat transfer |
| IV | Parallel-sheet | 10 | | Butt orientation, nine elements | Variation | Low | Maximum and minimum heat transfer |
| V | | 11 | | | Variation | High | |
| VI | Parallel-sheet | 12 | | 12° orientation, nine elements | Variation | Peak | Maximum and minimum heat transfer |
| VII | Triplet | 13 to 15 | | Butt orientation, nine elements | Reference | Peak | Maximum and minimum heat transfer |
| VIII | | 14 | | | Variation | Low | |
| IX | | 15 | | | Variation | High | |
| X | Triplet | 16 and 17 | | Single, large element | Reference | Peak | Maximum and minimum heat transfer |
| XI | | 16 | | | Variation | Low | |
| XII | | 17 | | | Variation | High | |

E-573

CG-3 back

TABLE II. - COMPARISON OF LIQUID-OXYGEN

AND HEPTANE VAPORIZATION RATES AT

VARIOUS CHAMBER LENGTHS[a]

| Chamber length, in. | Liquid oxygen vaporized, percent | Heptane vaporized, percent |
|---|---|---|
| 1 | 47 | 27 |
| 2 | 73 | 49 |
| 3 | 82 | 61 |
| 4 | 90 | 69 |
| 5 | 94 | 75 |
| 6 | 97 | 80 |
| 7 | 98 | 83 |

[a]Initial drop sizes, initial drop
velocities, and final gas velocities
of both propellants were equal. In-
itial temperatures of both propel-
lants were typical of actual rocket
firing conditions. Chamber pressure,
300 lb/sq in.

TABLE III. - SYSTEM FOR LABELING

THERMOCOUPLE ROW LOCATIONS

| Symbol | Thermocouple row locations | Curve connecting data points |
|---|---|---|
| O | Nonspray wall segments, reference case | Solid |
| ◖ | Nonspray wall segments, variation case | Dotted |
| □ | Spray wall segments, reference case | Solid |
| ◇ | Spray wall segments, variation case | Dotted |
| △ ◿ | Midway between spray and non-spray wall segments, varia-tion case | Dotted |

TABLE IV. - CALCULATED WALL TEMPERATURES

| Case | Local wall temperature, $(T_w)_{local}$, $^\circ F$ | |
|------|------------------------|------------------------|
| | Spray wall segments | Nonspray wall segments |
| I | 171 | 281 |
| II[a] | 205 (upper) | 197 (lower) |
| III | 117 | 210 |
| IV | 193 | 250 |
| V | 135 | 228 |
| VI | 226 | 216 |
| VII | 419 | 338 |
| VIII | 204 | 227 |
| IX | 266 | 266 |
| X | 158 | 229 |
| XI | 170 | 121 |
| XII | 136 | 142 |

[a]Thermocouple rows were located midway
between spray and nonspray regions;
therefore, they were equally affected
by propellant sprays. The "upper"
and "lower" notations refer to the
thermocouple row locations as shown
in the sketch of case II in fig. 8.

C-44103
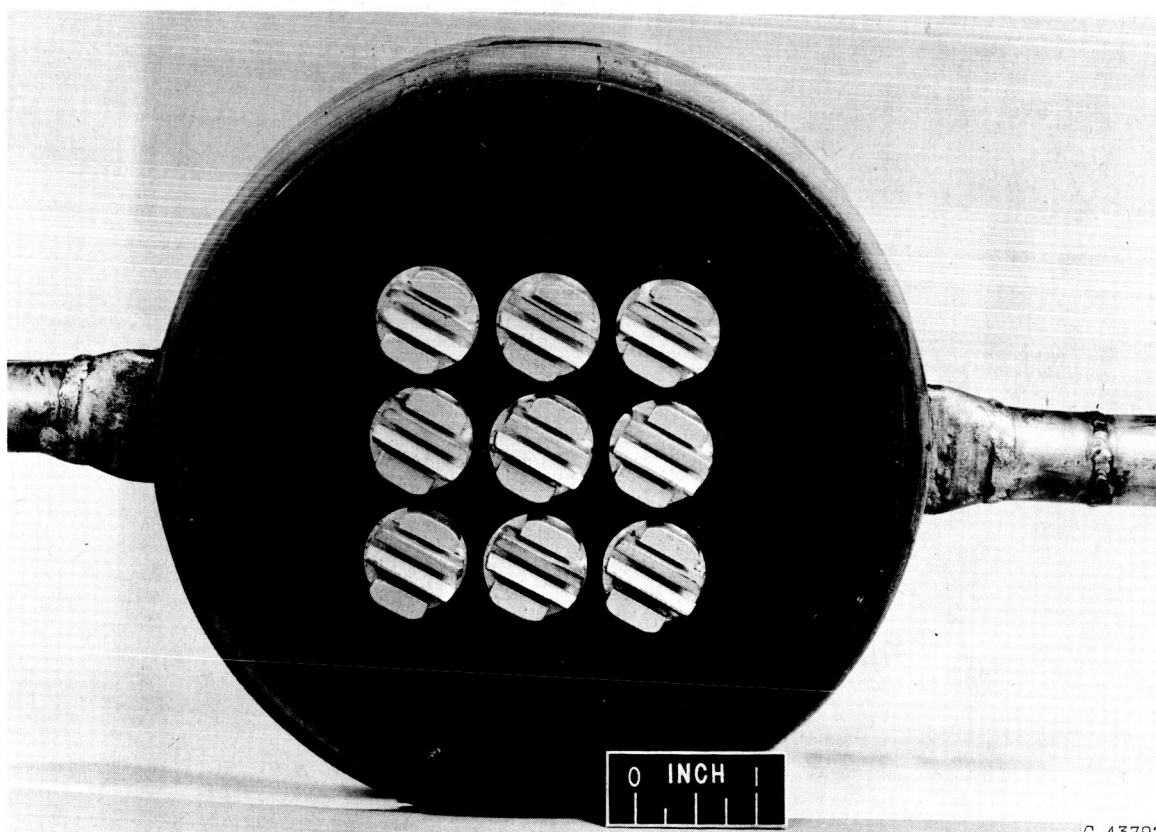


C-43792

Figure 1. - Unassembled and assembled views of parallel-sheet injector.
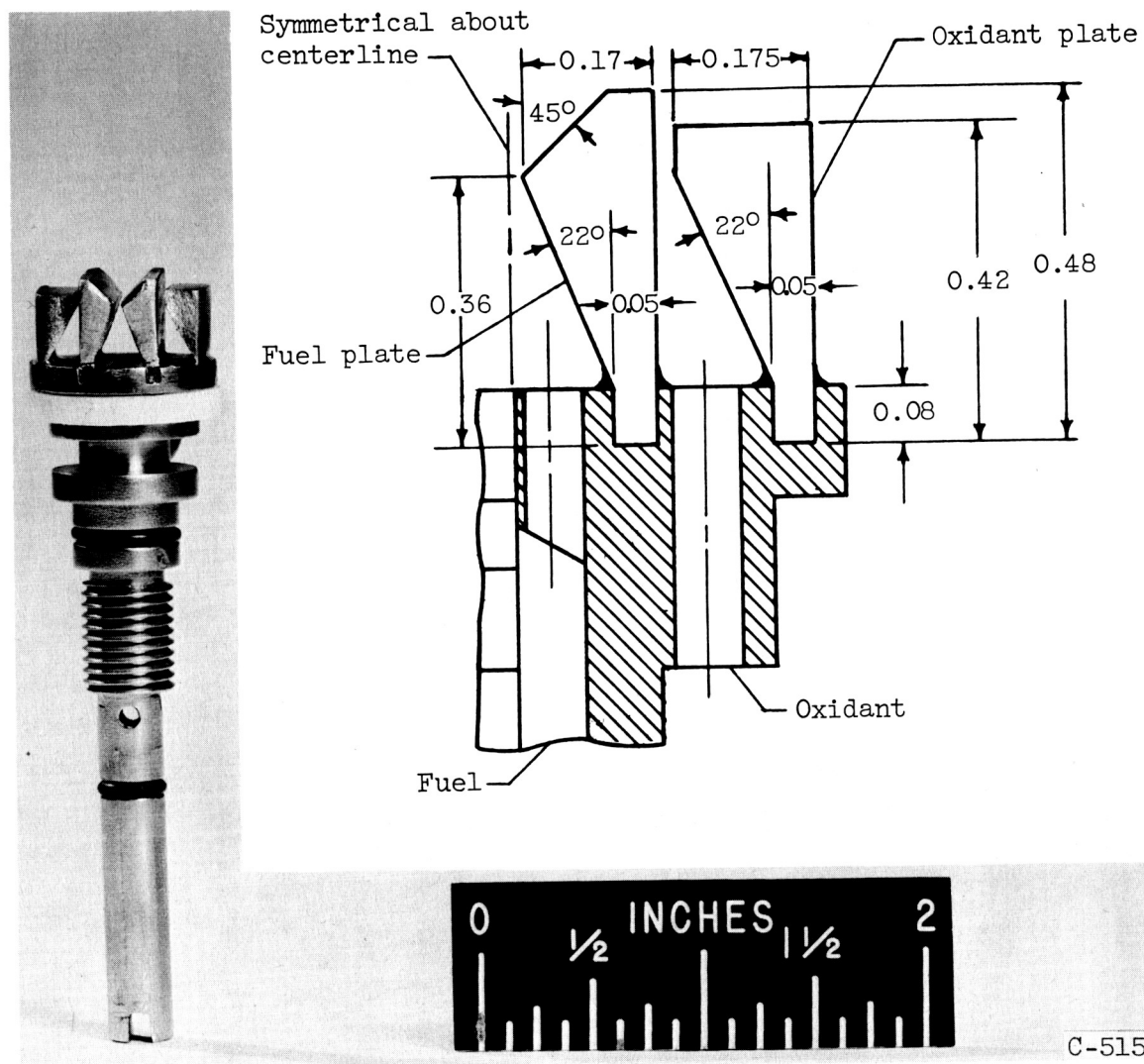
Figure 2. - Parallel-sheet element (dimensions in inches except where noted).
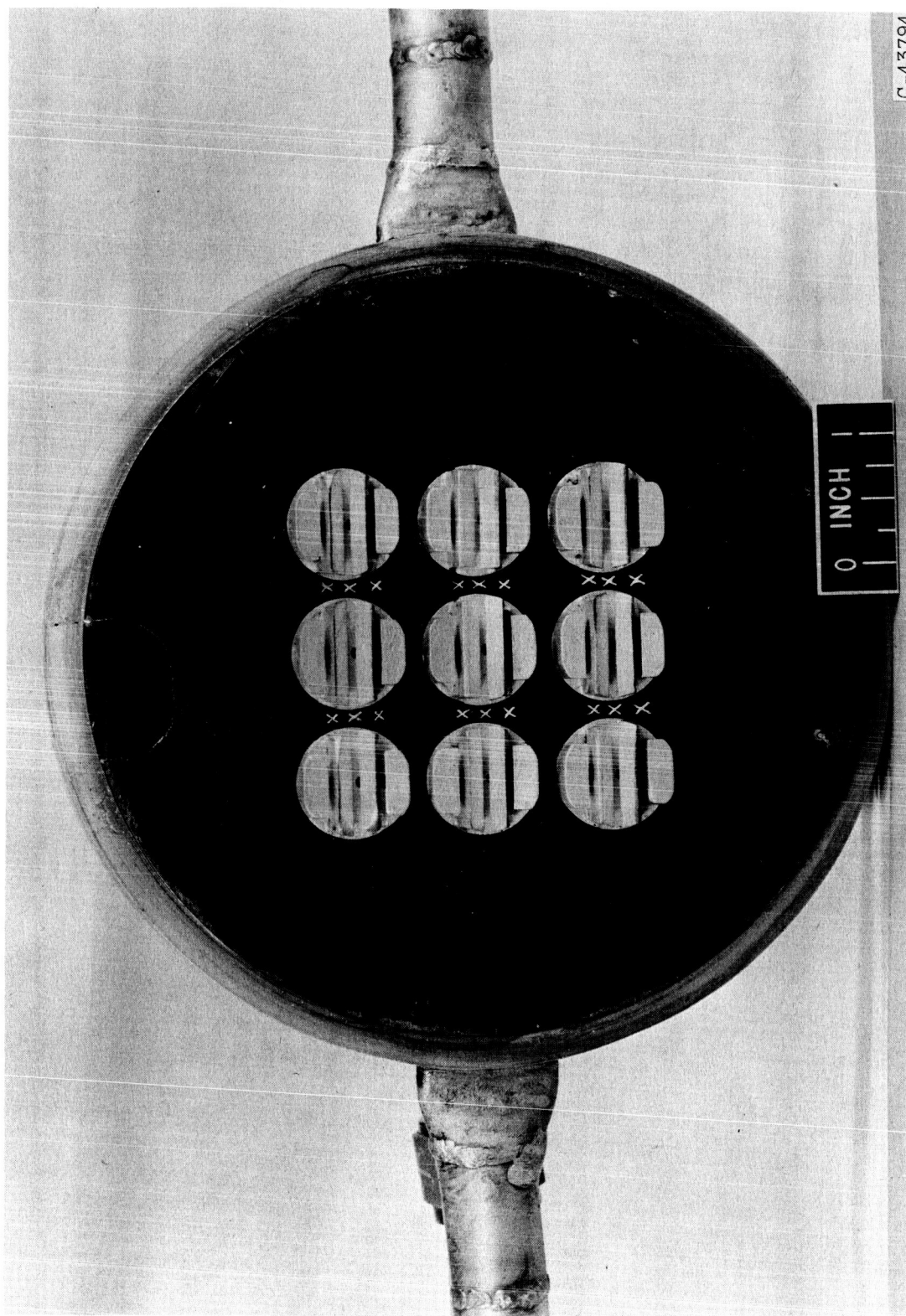
C-43794



Figure 3. - Nine-unit parallel-sheet injector with butt orientation. Total number of interference zones (denoted by X), 18.
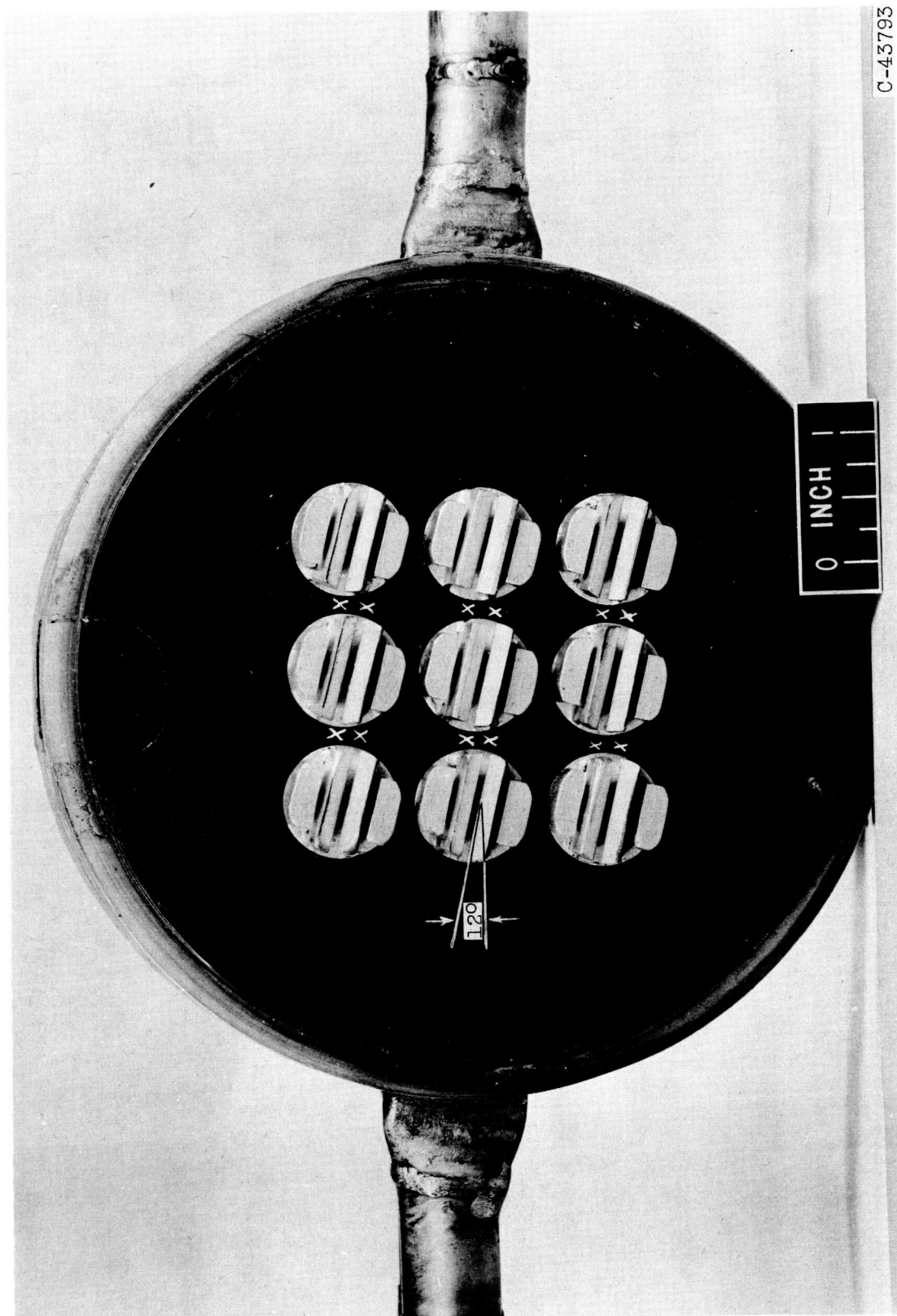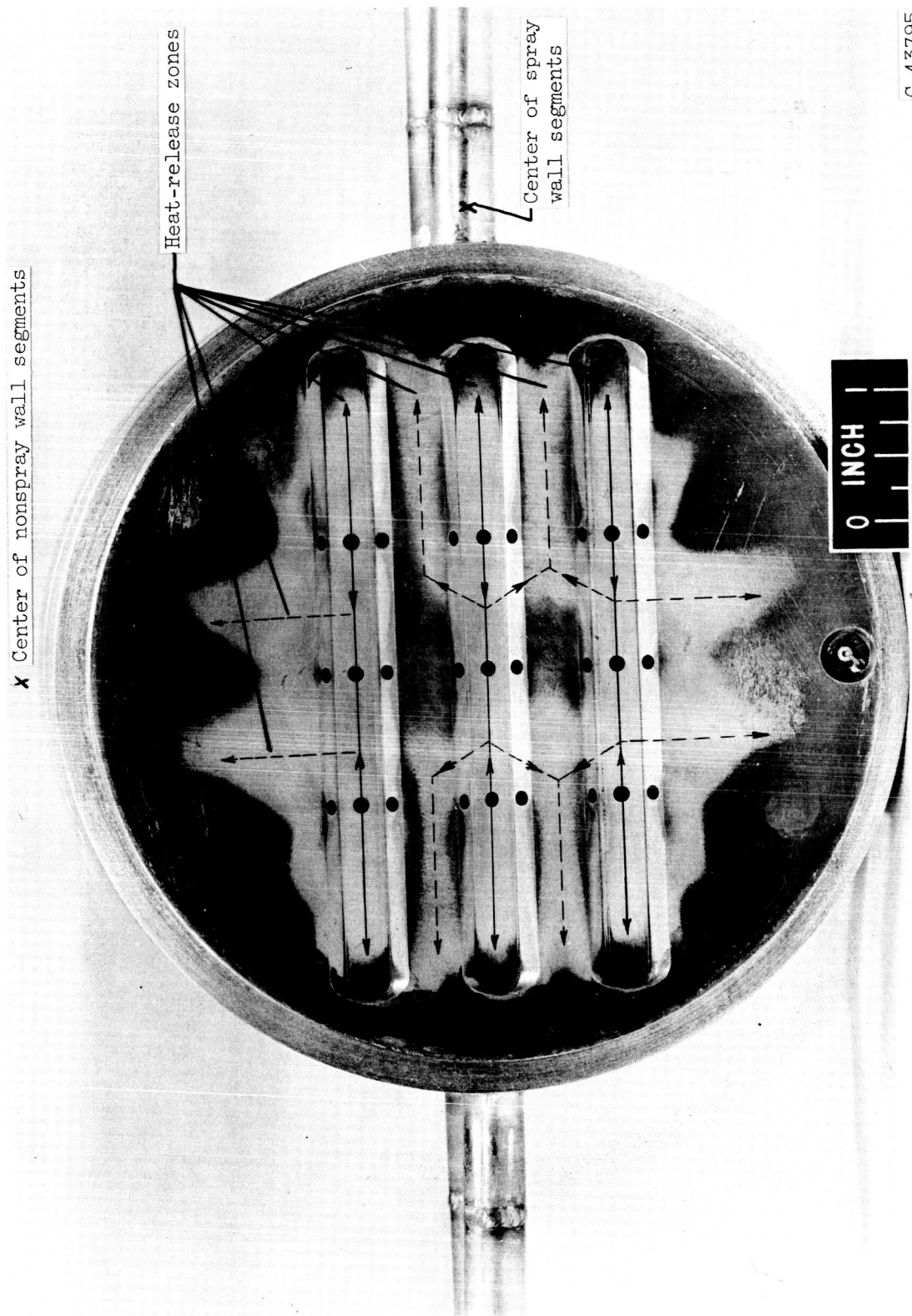
Figure 4. - Nine-unit parallel-sheet injector with 12° orientation. Total number of interference zones (denoted by X), 12.

E-573

C-43793

E-573

CG-4



**x** Center of nonspray wall segments

Heat-release zones

Center of spray wall segments

C-43795

Figure 5. - Fixed-element, nine-unit triplet injector with elements in butt orientation.
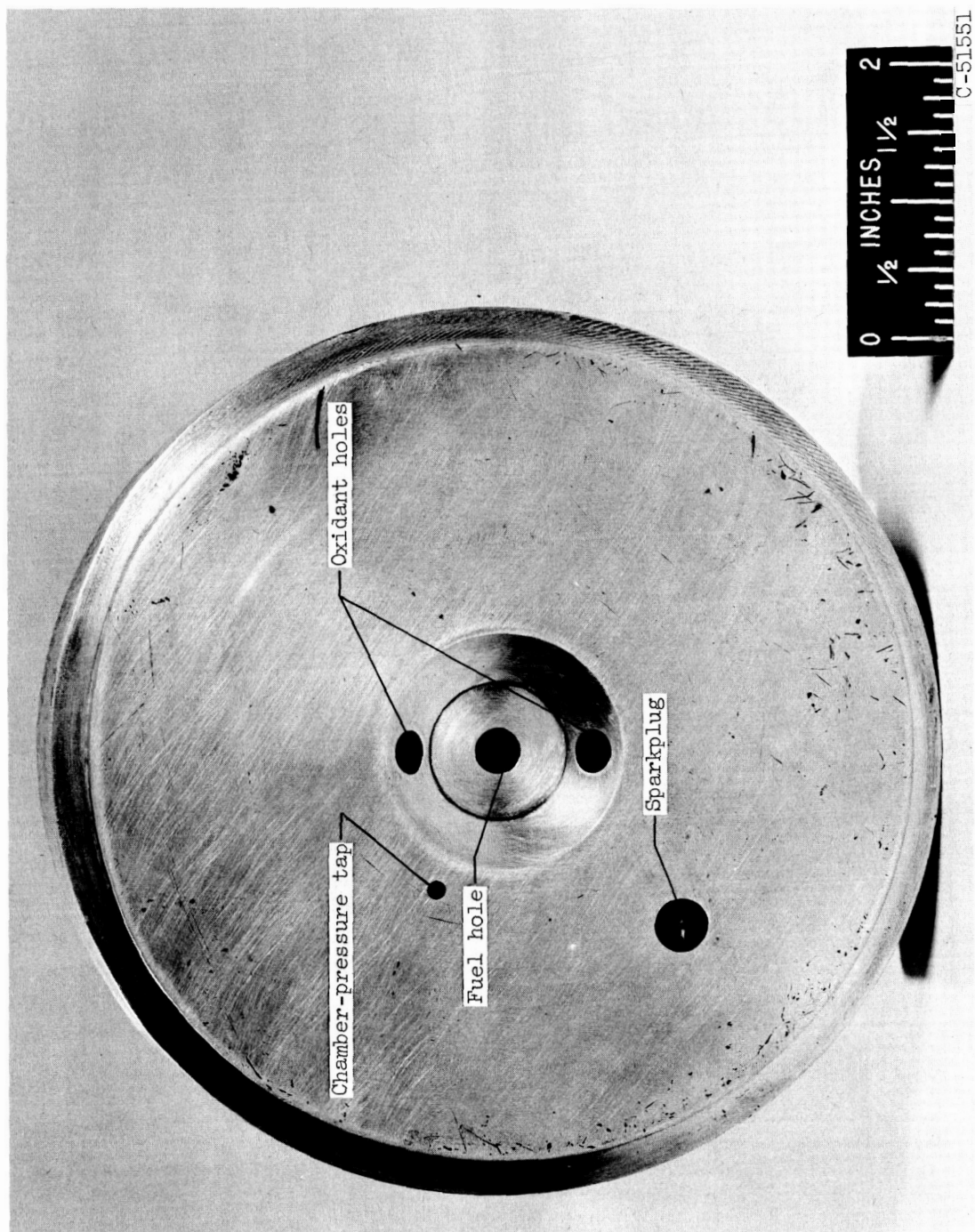
Figure 6. - Single-unit triplet injector.

E-573
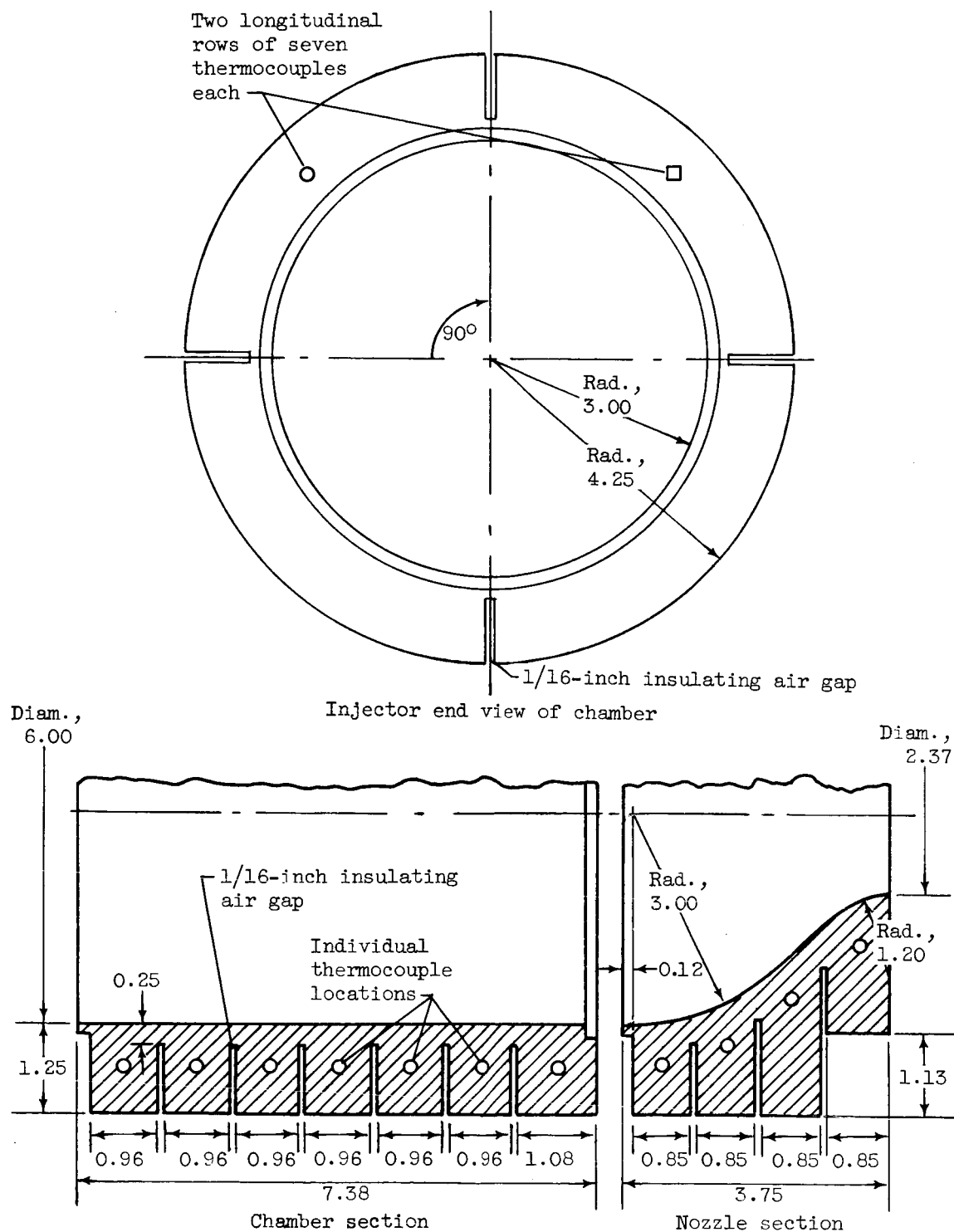
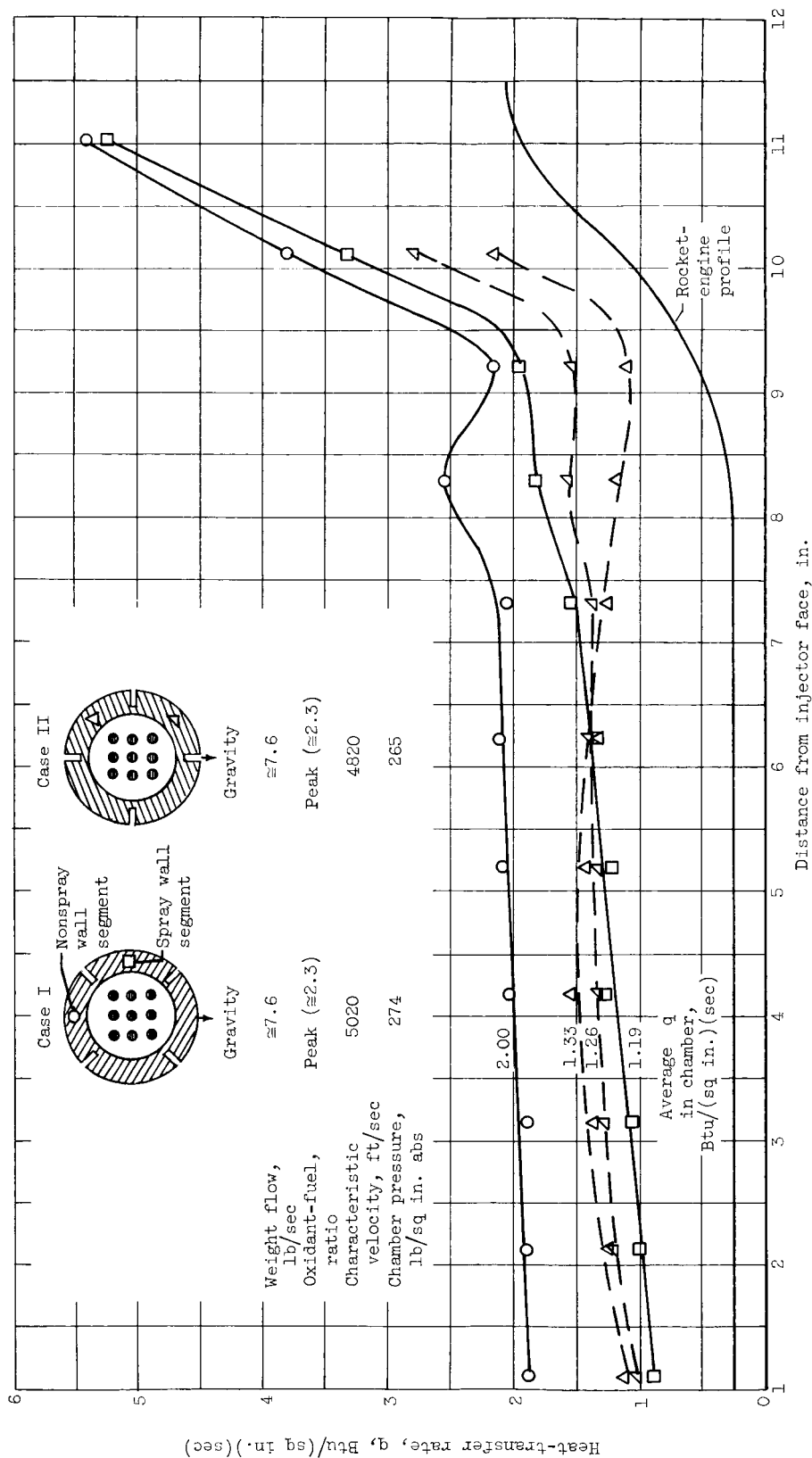Figure 7. - Schematic drawing of solid-copper segmented engine showing thermo-
couple locations (dimensions in inches).

Figure 8. - Localized heat-flux rates at four circumferential positions.  Parallel-sheet injector with butt orientation.
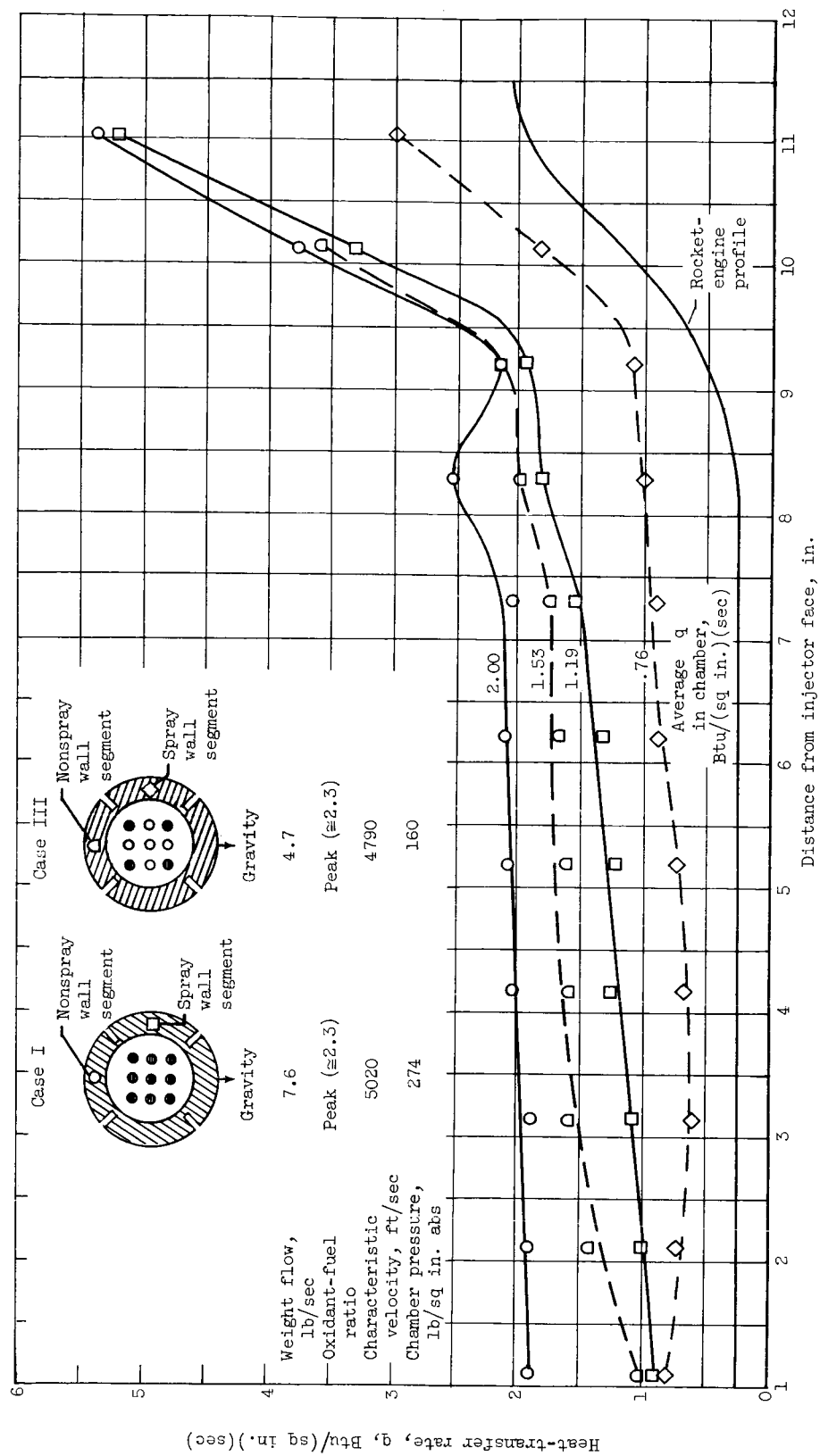
E-573



Figure 9. - Localized heat-flux rates at two propellant flow rates and chamber pressures. Parallel-sheet injector with butt orientation.
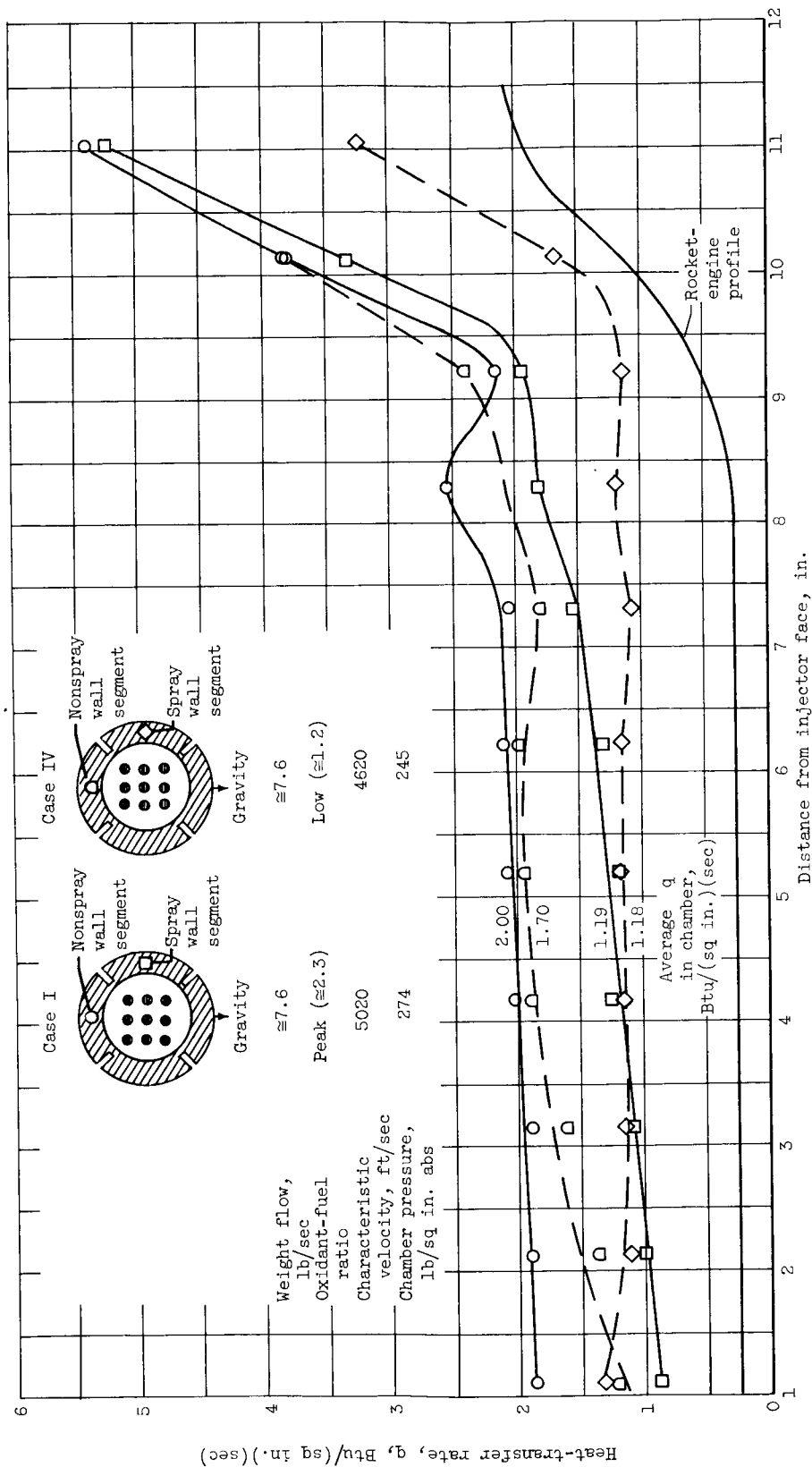
Heat-transfer rate, q, Btu/(sq in.)(sec)

Distance from injector face, in.

|  | Case I | Case III |
|---|---|---|
| Weight flow, lb/sec | 7.6 | 4.7 |
| Oxidant-fuel ratio | Peak (≅2.3) | Peak (≅2.3) |
| Characteristic velocity, ft/sec | 5020 | 4790 |
| Chamber pressure, lb/sq in. abs | 274 | 160 |

Nonspray wall segment

Spray wall segment

Gravity

Rocket-engine profile

Average q in chamber, Btu/(sq in.)(sec)

2.00

1.53

1.19

.76

Figure 10. - Localized heat-flux rates at peak and low oxidant-fuel ratios. Parallel-sheet injector with butt orientation.
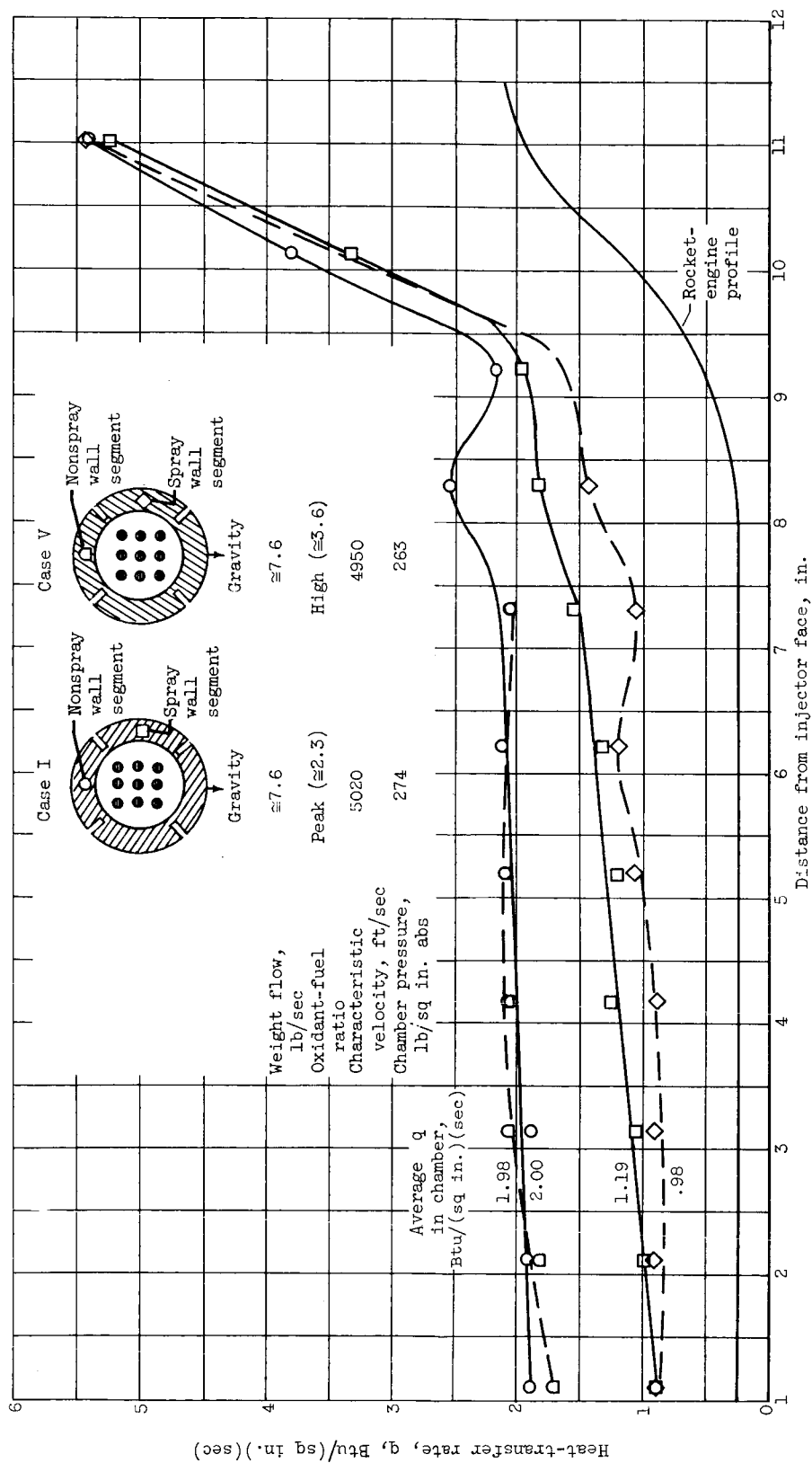
E-573



Figure 11. - Localized heat-flux rates at peak and high oxidant-fuel ratios. Parallel-sheet injector with butt orientation.
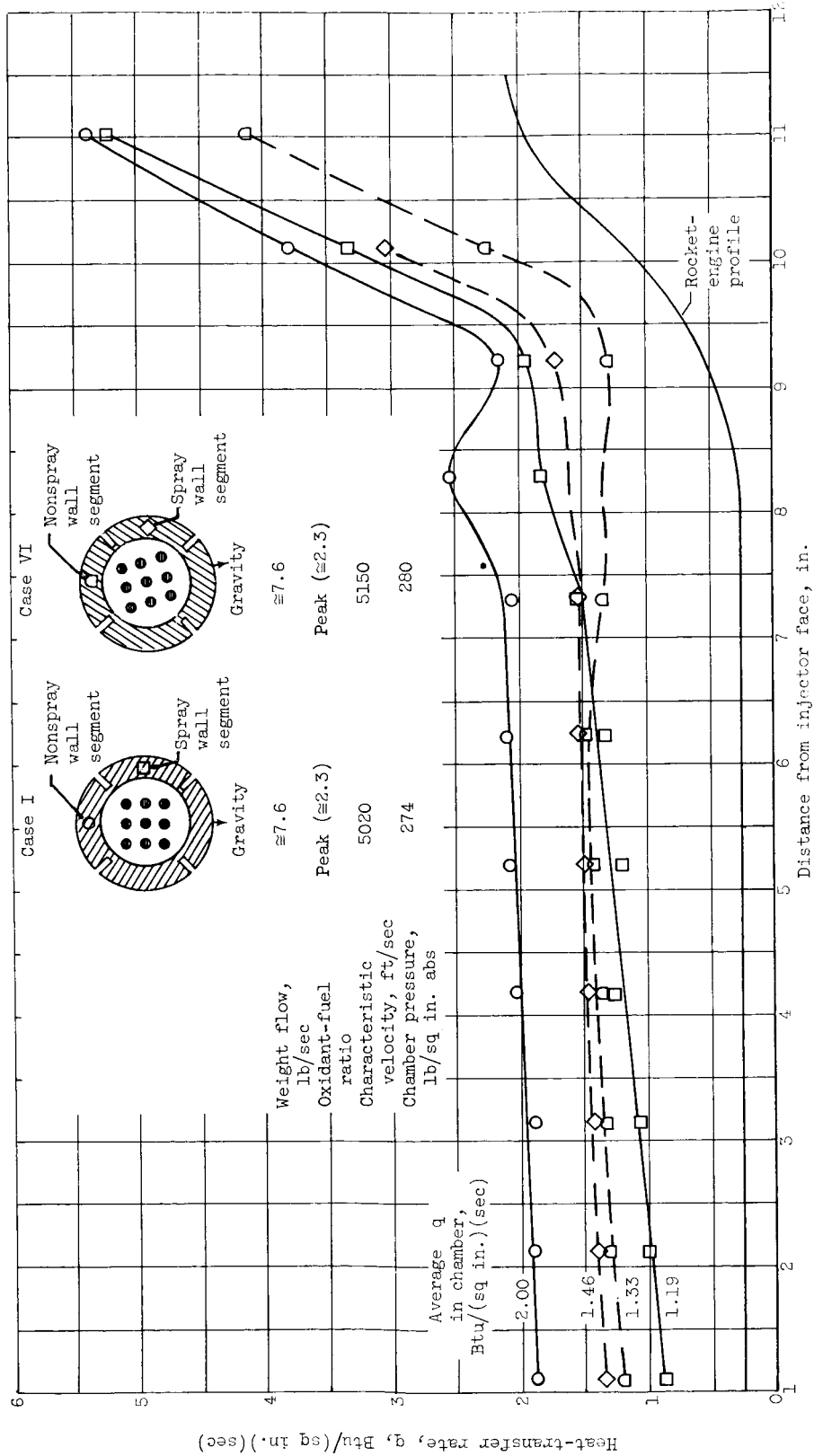
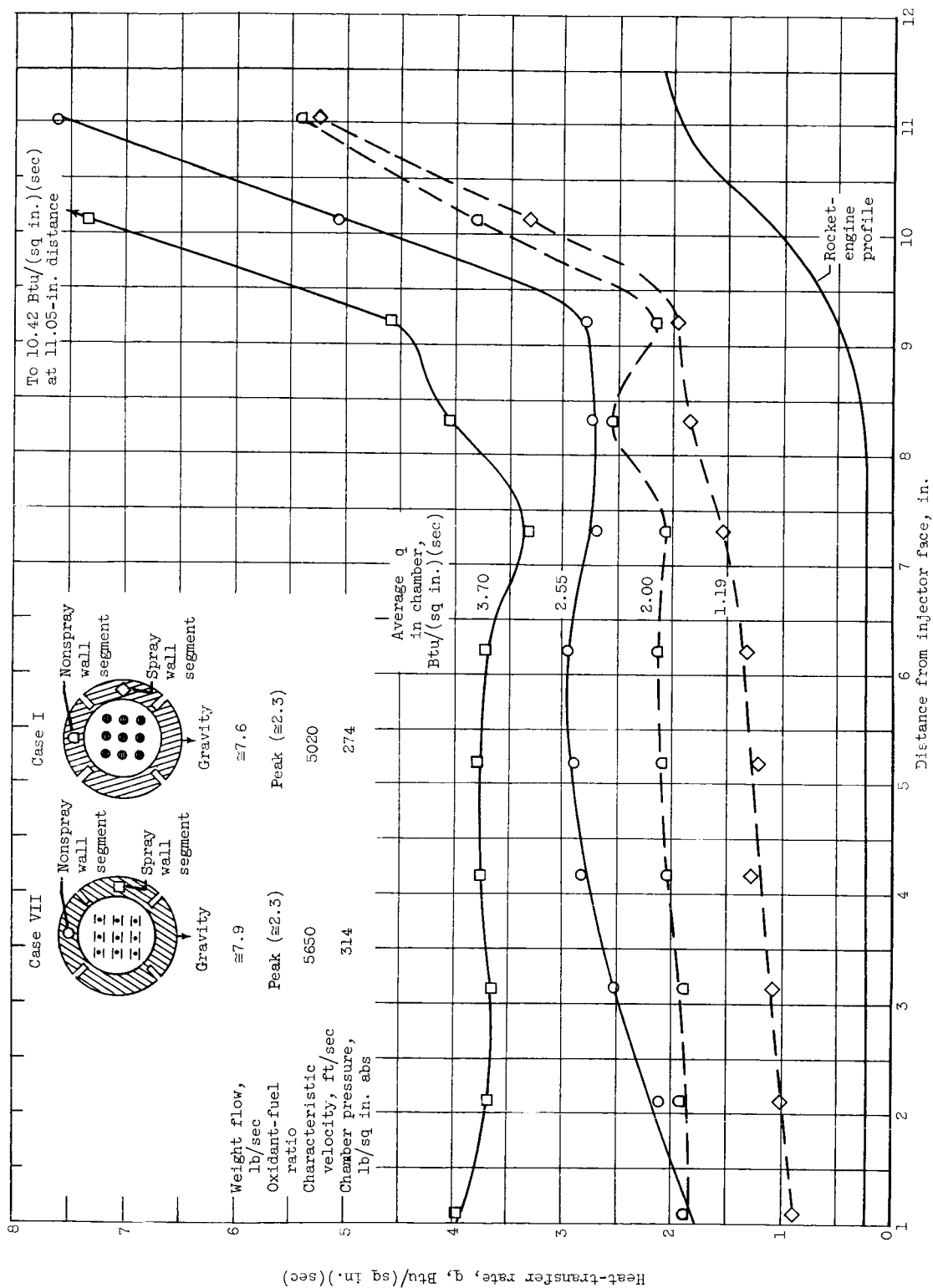Figure 12. - Localized heat-flux rates for butt and 12° orientations of parallel-sheet injector inserts.

Figure 13. - Localized heat-flux rates for parallel-sheet and nine-element-triplet injectors at peak oxidant-fuel ratio.
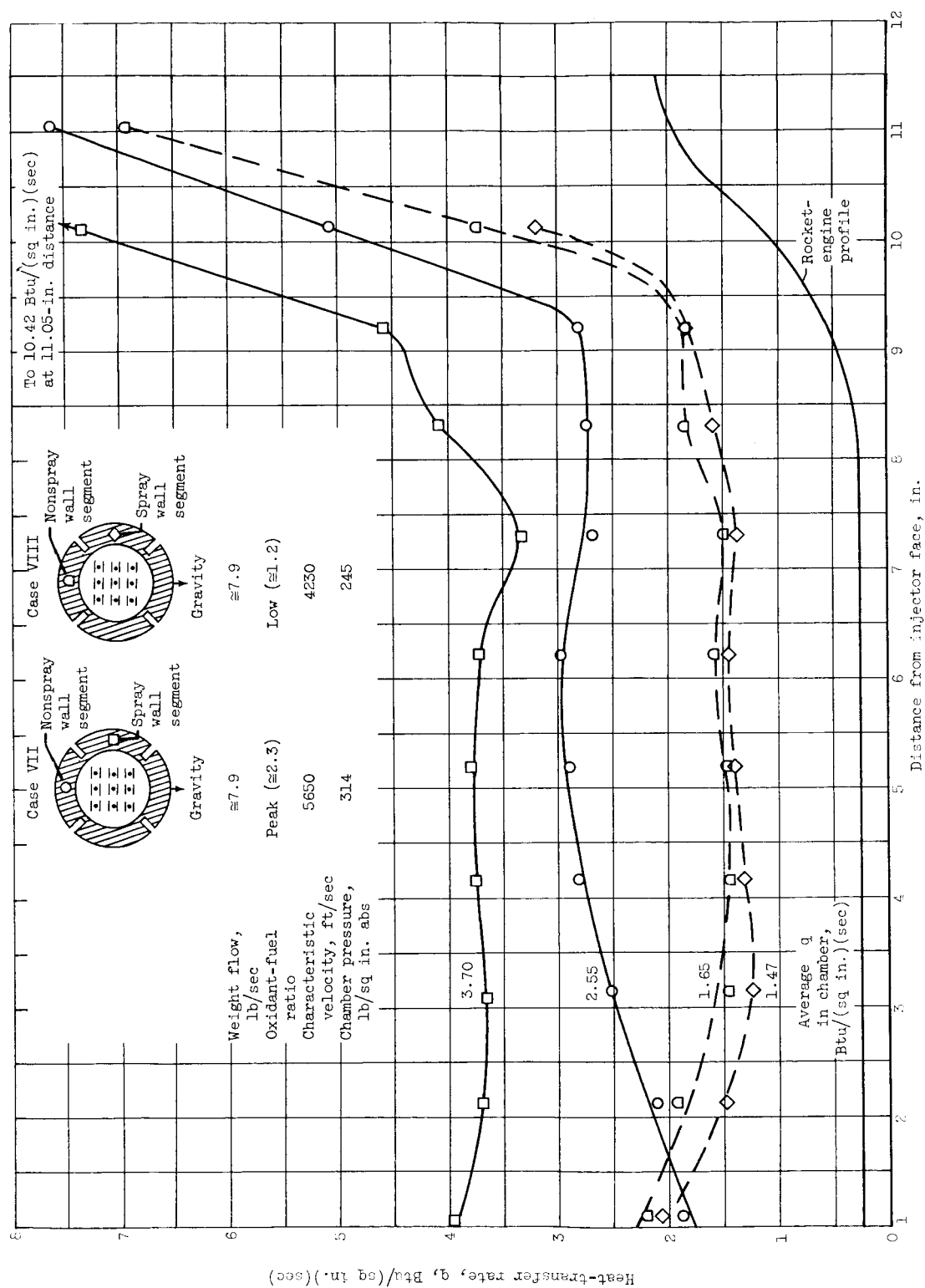
34

E-573

To 10.42 Btu/(sq in.)(sec)
at 11.05-in. distance

| | Case VII | Case VIII |
|---|---|---|
| | Nonspray wall segment / Spray wall segment / Gravity | Nonspray wall segment / Spray wall segment / Gravity |
| Weight flow, lb/sec | ≅7.9 | ≅7.9 |
| Oxidant-fuel ratio | Peak (≅2.3) | Low (≅1.2) |
| Characteristic velocity, ft/sec | 5650 | 4230 |
| Chamber pressure, lb/sq in. abs | 314 | 245 |

3.70

2.55

1.65

1.47

Average q in chamber, Btu/(sq in.)(sec)

Rocket-engine profile

Distance from injector face, in.

Heat-transfer rate, q, Btu/(sq in.)(sec)

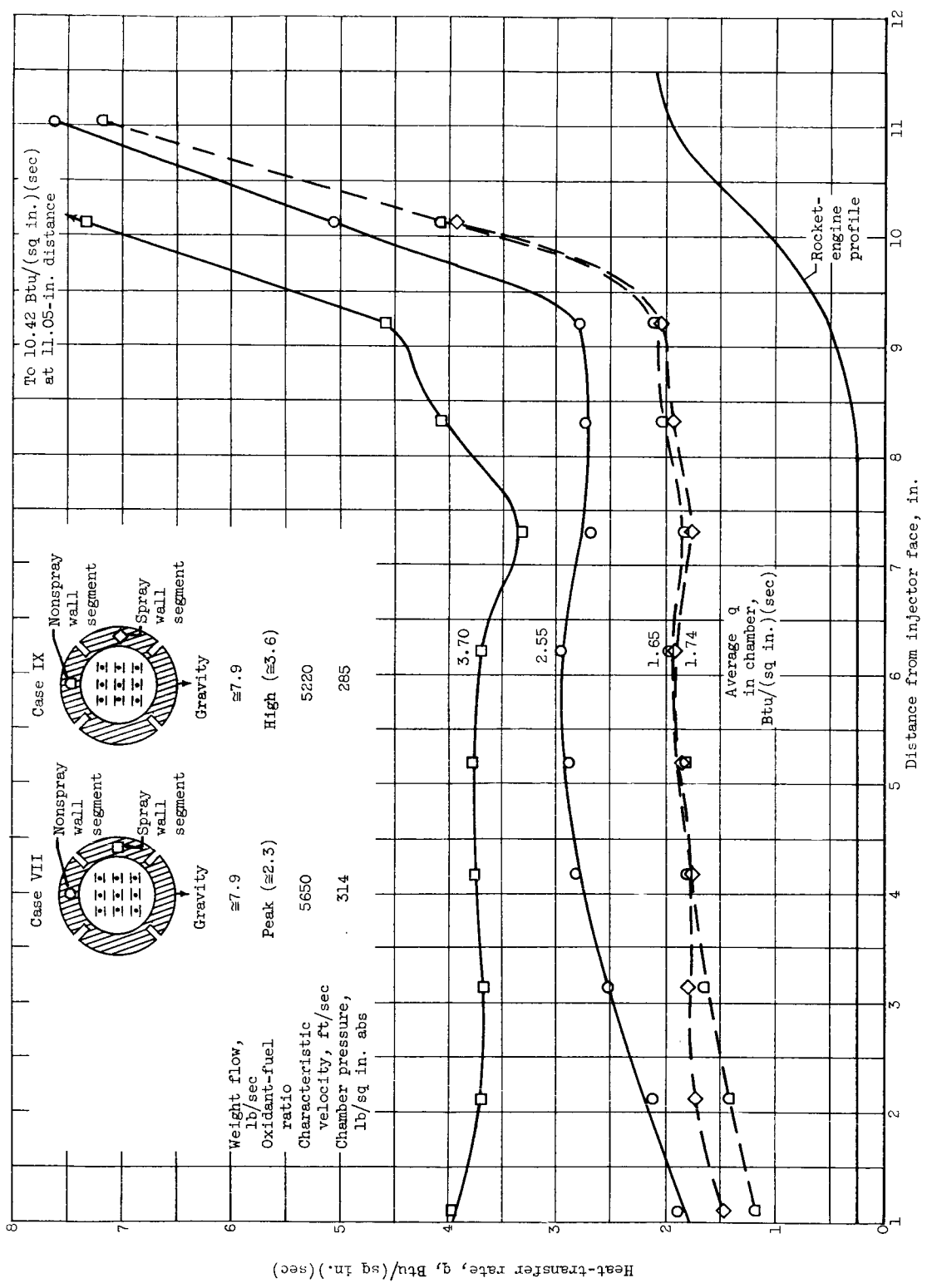Figure 14. - Localized heat-flux rates for nine-element-triplet injector at peak and low oxidant-fuel ratios.

E-573

CG-5 back



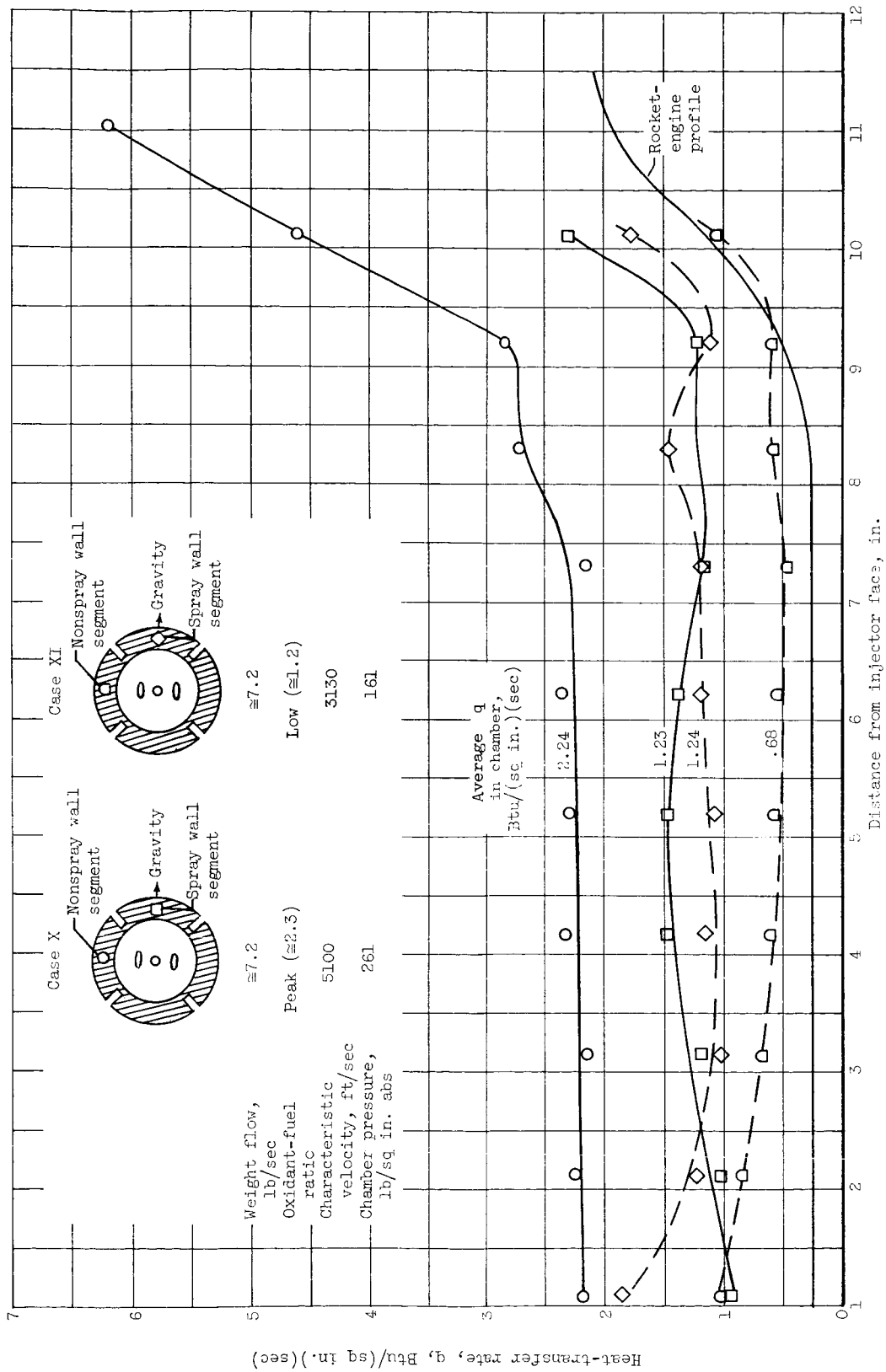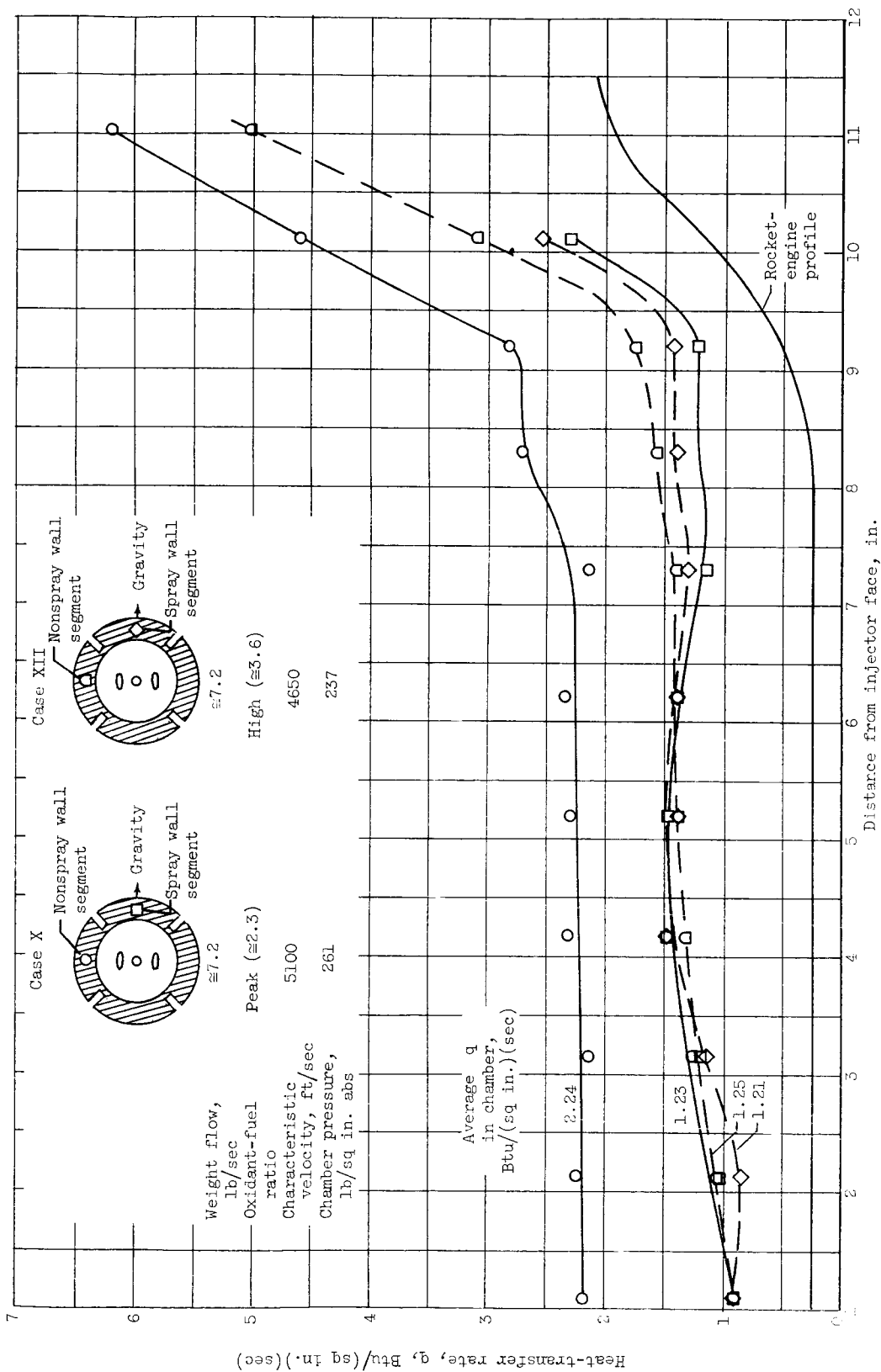Figure 15. - Localized heat-flux rates for nine-element-triplet injector at peak and high oxidant-fuel ratios.

Heat-transfer rate, q, Btu/(sq in.)(sec)

Distance from injector face, in.

Rocket-engine profile

|  | Case X | Case XI |
|---|---|---|
| Weight flow, lb/sec | ≅7.2 | ≅7.2 |
| Oxidant-fuel ratio | Peak (≅2.3) | Low (≅1.2) |
| Characteristic velocity, ft/sec | 5100 | 3130 |
| Chamber pressure, lb/sq in. abs | 261 | 161 |

Nonspray wall segment
Gravity
Spray wall segment

Average q in chamber, Btu/(sq in.)(sec)

2.24

1.23

1.24

.68

Figure 16. - Localized heat-flux rates for single-element-triplet injector at peak and low oxidant-fuel ratios.

Figure 17. - Localized heat-flux rates for single-element-triplet injector at peak and high oxidant-fuel ratios.

Figure 19. - Effect of oxidant-fuel ratio on specific heat for liquid-oxygen - heptane propellant combination. Chamber pressure, 300 pounds per square inch; obtained from unpublished NASA data.
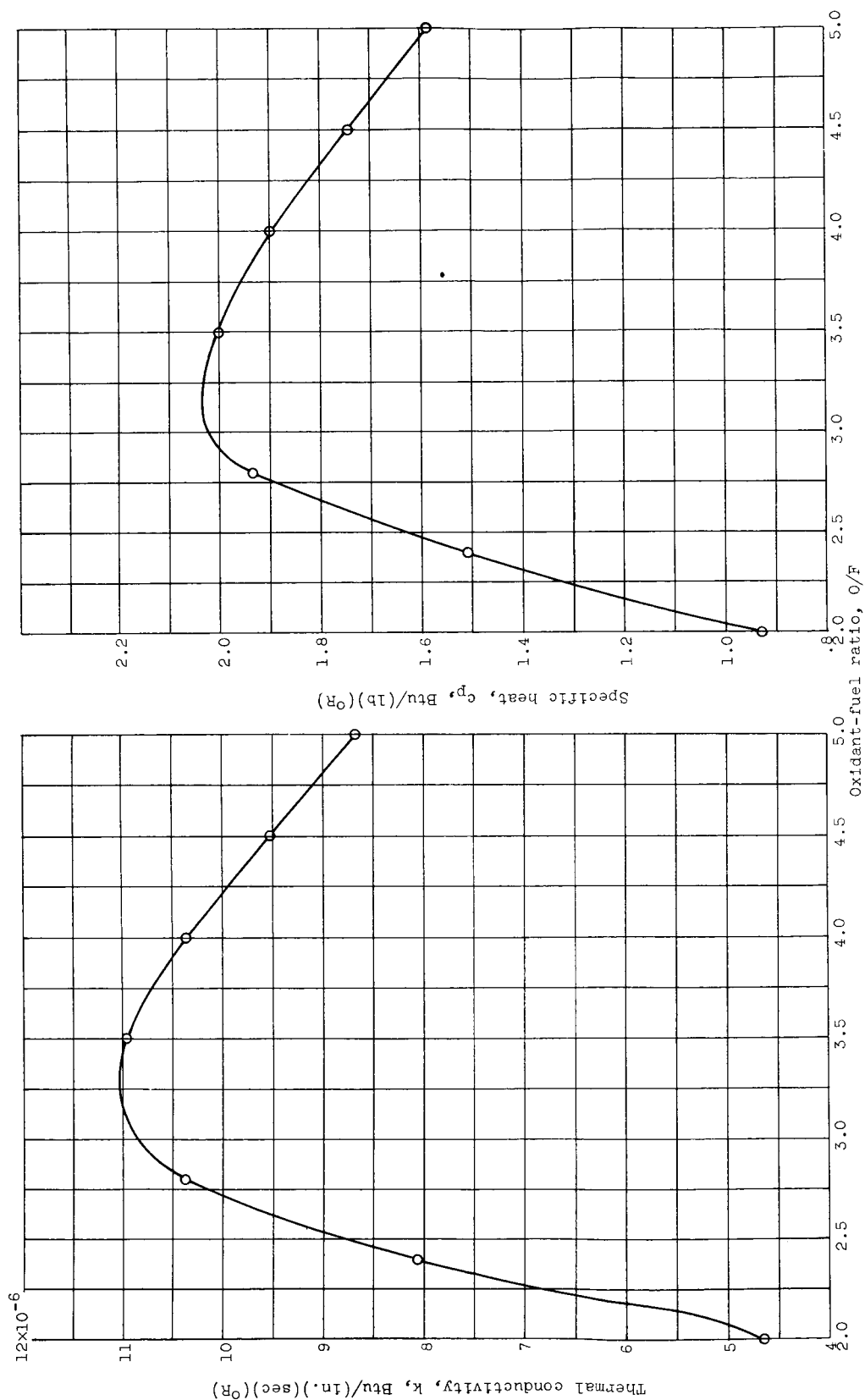


Figure 18. - Effect of oxidant-fuel ratio on thermal conductivity for liquid-oxygen - heptane propellant combination. Chamber pressure, 300 pounds per square inch; obtained from unpublished NASA data.

E-575

E-573



Figure 21. - Effect of oxidant-fuel ratio on combustion gas temperature for the liquid-oxygen - heptane propellant combination. Chamber pressure, 300 pounds per square inch; obtained from unpublished NASA data.
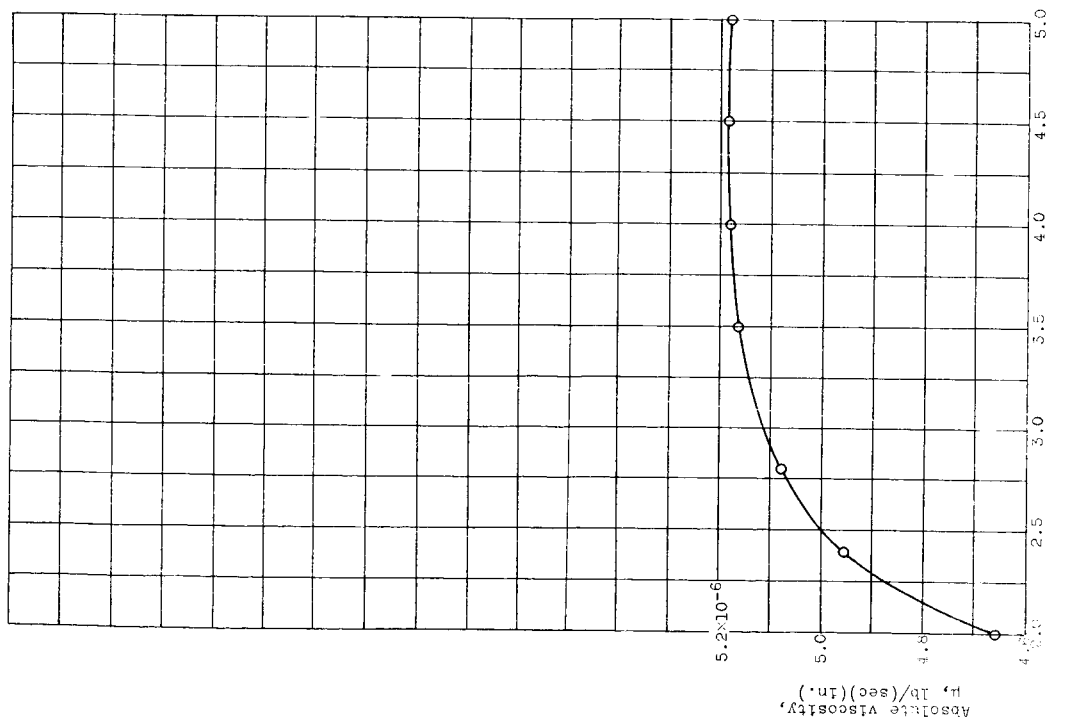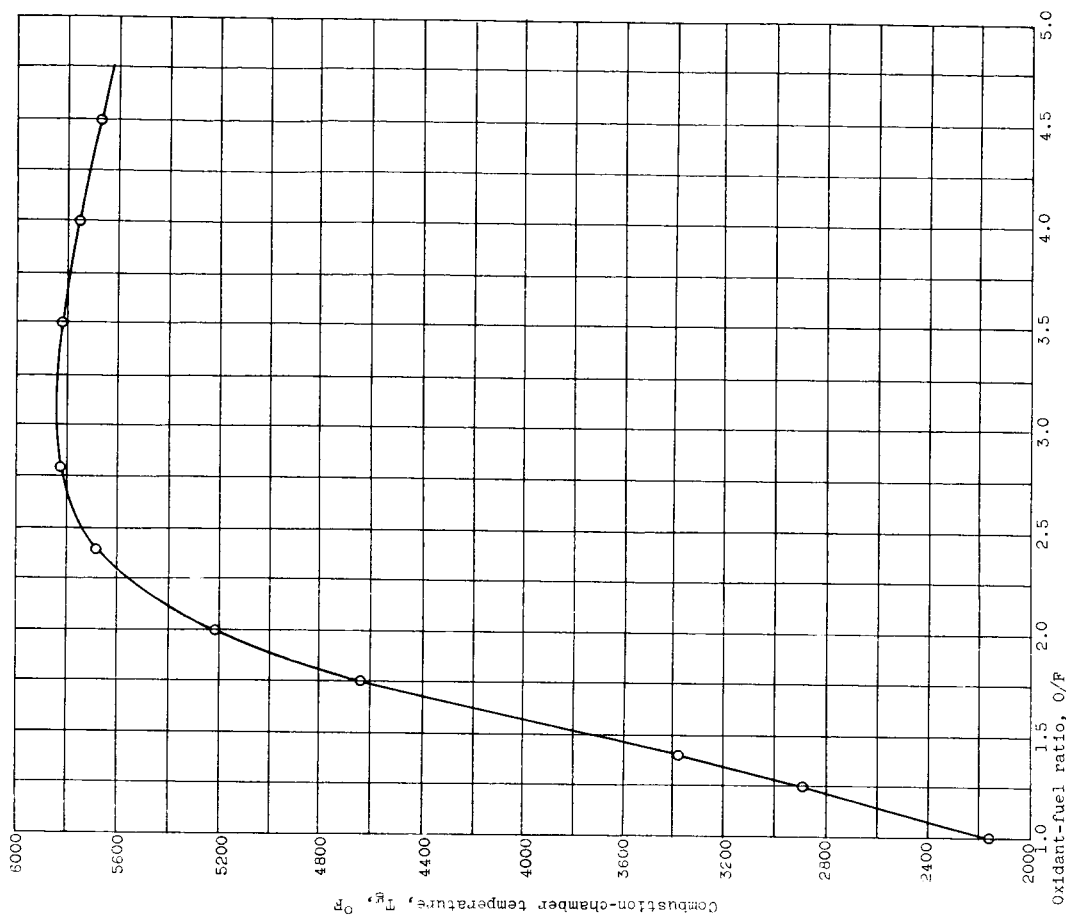


Figure 20. - Effect of oxidant-fuel ratio on absolute viscosity for the liquid-oxygen - heptane propellant combination. Chamber pressure, 300 pounds per square inch; obtained from unpublished NASA data.